The Resistance Committee

Final Report and Recommendations to the 28th ITTC

1 INTRODUCTION

1.1 Membership and Meetings

The members of the Resistance Committee of the 28th ITTC are:

- Dr. Thomas C. Fu (Chair)
  Office of Naval Research,
  Ship Systems and Engineering Research Division
  Arlington, Virginia, U.S.A.

- Dr. Hisao Tanaka
  Japan Marine United Corporation
  Tsu, Japan

- Dr. Jin Kim
  Maritime and Ocean Engineering
  Research Institute
  Daejeon, Korea

- Assoc. Prof. Gregor Macfarlane
  Australian Maritime College
  University of Tasmania
  Tasmania, Australia

- Wentao Wang
  China Ship Scientific Research Center
  China

- Dr. Richard Pattenden
  QinetiQ
  United Kingdom

- Dr. Mario Felli
  CNR-INSEAN
  Rome, Italy

- Professor Sakir Bal
  Istanbul Technical University
  Istanbul, Turkey

Four committee meetings have been held during the work period:

- Washington, DC, USA, 3–4 March 2015 at Naval Surface Warfare Center, Carderock Division.

- Tokyo, Japan, 30 Nov—1 Dec 2015, at National Maritime Research Institute

- Gosport, England, 26–27 July 2016, at QinetiQ

- Launceston, Tasmania, 16 – 17 February 2017 at Australian Maritime College.

1.2 Tasks

The recommendations for the work of the Resistance Committee as given by the 27th ITTC were as follows:

(1) Update the state-of-the-art for predicting the resistance of different ship concepts emphasizing developments since the 2014 ITTC Full Conference. The committee report should include sections on:

a. The potential impact of new technological developments on the ITTC.
b. New experimental techniques and extrapolation methods.
c. New benchmark data.
d. The practical applications of computational methods to resistance predictions and scaling.

e. The need for R&D for improving methods of model experiments, numerical modeling and full-scale measurements.

(2) During the first year, review ITTC Recommended Procedures relevant to resistance and resistance specific CFD procedures:

a. Identify any requirements for changes in the light of current practice, and, if approved by the Advisory Council, update them.

b. Identify the need for new procedures and outline the purpose and content of these.

(3) Review definitions of ship surface roughness and develop a guideline for its measurement; hereunder resolve differences between ISO 4287 and the widely used BMT roughness measurement system. Include the effect of coatings and their through-life changes.

(4) Review trends and new developments on understanding the phenomenon of unsteady free surface flows, including their influence on added resistance and experimental techniques

(5) Develop a new procedure for wave profile measurement and wave resistance analysis.

(6) Review roughness of models and appendages produced by rapid prototyping. Assess effects of this roughness on resistance.

(7) Propose guidance for ITTC members to reduce/manage their uncertainty as a result of the worldwide resistance benchmark tests of previous ITTCs.

(8) Review turbulence stimulation methods and devices from the point of view of their physics and update the relevant procedure 7.5-01-01-01 Ship models. Check occurrence of turbulence stimulation methods in other procedures and update as needed.

(9) Develop a procedure for verification and validation of the detailed flow field data.

(10) An ITTC benchmark study shall be initiated according to 7.5-01-03-04 Benchmark for PIV (2C) and SPIV (3C) set-ups. The benchmark study would involve PIV measurements performed on a flow of interest, with fully detailed uncertainty analysis. The results can then be compared with similar measurements done in different facilities or with high-quality CFD computations from various organizations.

(11) Continue the World Wide Campaign and endeavour to obtain the new and already submitted test data in open form in order to enable a more detailed insight into the deviations between the data.

2 STATE OF THE ART

2.1 Experimental Techniques and Extrapolation

The most notable and organized activity on experimentation topics in the marine environment is the Advanced Model Measurement Technology conference series (AMT). The 5th conference of the series, held in Istanbul in September 2015, gives specific emphasis on coating assessment and performance, drag reduction and energy efficiency of ships.

New experimental approaches have been proposed to collect and monitor biofilm growth and assess their effect on the frictional drag characteristics. Atlar et al. (2015) reported on the design, manufacture and early operational experiences of a specially designed strut arrangement deployed on the research vessel of Newcastle University to collect fouling samples while the ship in in-service (Figure 1).Demirel et al. (2015) presented a novel experimental approach to predict the added resistance caused by the calcareous fouling. The approach is

based on an extensive series of towing tests in which the effects of the coverage percentage and locations of the fouling accumulation is examined over a range of Reynolds numbers using flat plates covered with artificial, 3D printed barnacles. Li et al. (2015) measured the roughness characteristics of a biofilm cultivated in a controlled environment and assessed its effect on the frictional drag characteristics using a special axisymmetric body apparatus.

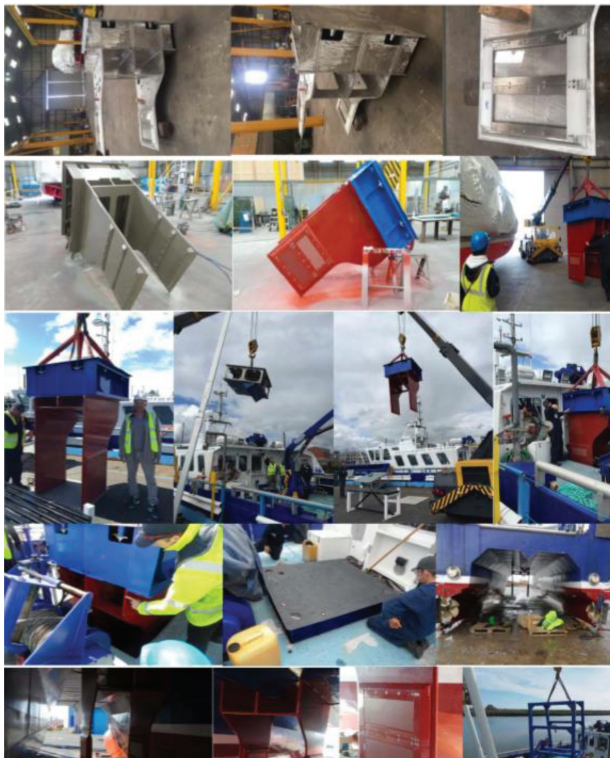

Figure 1 Manufacturing, painting, initial installation process and some details of the moon pool plug and strut assembly as well as transporting of safe stand (Time sequence of events is left to right and from top to bottom) (Atlar et al., 2015)

The use of convectional approaches based on resistance measurements has been improved through dedicated apparatuses minimizing any interference and other uncertainty sources, included the human factor. For example, Perelman et al. (2015) used a dedicated balance designed to reject parasitic forces due to the cross coupling interference in the direction perpendicular to the flow to undertake high Reynolds skin friction tests about samples of smooth and rough surfaces, treated with several coating systems. Savio et al. (2015) performed resistance tests on a series of plates (6m × 0.6m), having different roughness levels, in fully automatic mode in order to carry out tests exactly in the same way for all the tested plates (i.e. the carriage is left unmanned and the tests are executed with prescribed automatic procedures).

Some advances have been made in the assessment of the roughness and coating application characteristics. For example, Li et al. (2015) used a tailor made portable laser profilometer which provides a contactless measurement capability of roughness characteristics by a laser probe installed on a traverse device, whose positioning relative to the test surface is measured by an encoder (Figure 2). Savio et al. (2015) measured roughness characteristics through a high resolution 3D scanning laser, making several imprints of each plate to cover a surface extent much bigger than the laser scanner area. Moving Gaussian and spatial filters (with different cut offs) were applied to the surface profiles to account for spatial distribution, to filter out various surface texture features and to remove the long wavelength "form" of the plate and its imprints (Figure 3). The accurate assessment of the coating application characteristics is a relevant issue in the execution of resistance tests since the performances of the same paint can be influenced significantly by the quality of the application, as reported in Savio et al. (2015). This implies that high quality surface scans, able to resolve minimal differences in the paint application should be used.

The development and application of new experimental approaches to measure the wall stress distribution has been mainly based on the use of optical techniques. For example, Olson et al. (2015) introduced a new non-intrusive surface pressure and shear stress diagnostics technique that works as the molecular counter-

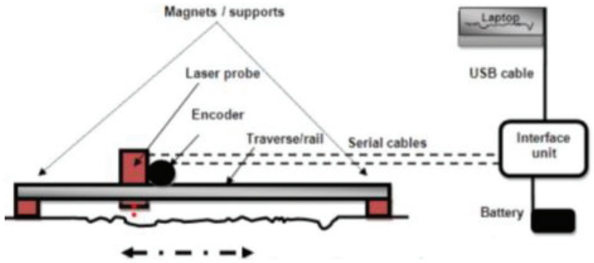

Figure 2 Portable laser profilometer schematic diagram (Li et al., 2015)

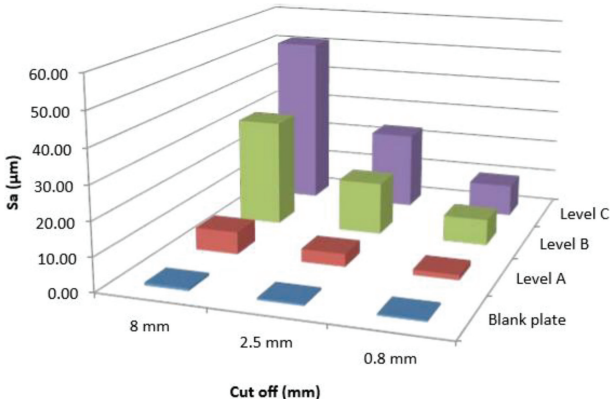

Figure 3 Arithmetic mean of absolute heights of the surface of the tested plates for three cut offs; 8, 2.5 and 0.8 mm (Savio et al., 2015)

part of Particle Image Velocimetry (PIV). In this technique, fluid molecules, rather than seed particles, are marked and tracked to enable wall-glare-free-boundary-layer-resolved measurements. Another approach concerns the use of Temperature Sensitive Paint (TSP) that relies on surface temperature measurements to obtain the relative skin friction characteristics (see Liu, 2013).

For testing catamarans in towing tanks, the concept of towing a single demihull in close proximity to the tank wall for taking interference effects into account was used by Zurcher et al. (2013), Kamal et al. (2015) and Haase et al. (2016b), as shown Figure 5. The advantage over the full catamaran configuration including both demihulls is that more physical space is available in the model for mounting equipment, such as self-propulsion gear and that larger scale factors can be achieved. Tank length and water depth may then become the limiting factors for the model size (Haase et al. 2016a). This concept was proven by Rovere (1997).

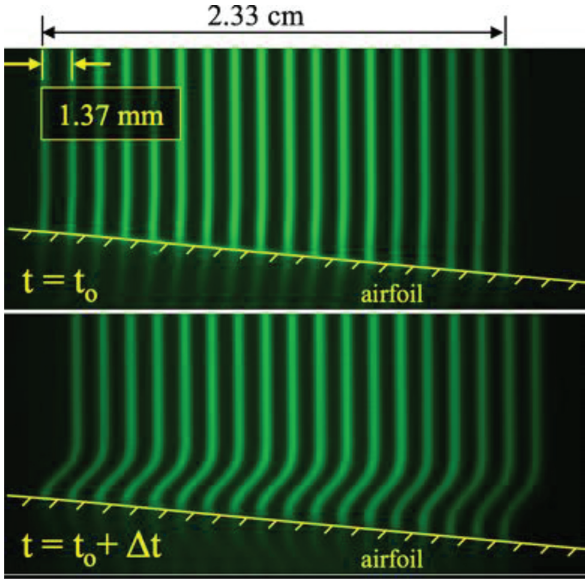

Figure 4 Example 1c-MTV image pair obtained over a portion of the suction surface of an airfoil at incidence: "undelayed" (top) and "delayed" (bottom) images are separated by 10 ms. Green lines represent phosphorescence produced by molecules excited by Excimer

2.2 New Benchmark Data

A new ship hull used in Tokyo 2015: A Workshop on CFD in Ship Hydrodynamics (http://www.t2015.nmri.go.jp) is a Capsized bulk carrier called Japan Bulk Carrier (JBC), which has been designed together with its energy saving duct for the validation of the CFD predictions of ship flows with energy saving device. The design ship speed is set to 14.5 knots. The propeller is a conventional five-bladed propeller with the AU section. The geometries of a main hull and a duct are shown in Figure 6 and the principal particulars are listed in Table 1 and Table 2. The duct has a circular shape with the diameters of 0.55 D_p(propeller diameter), the angle of attack 20 Deg. And its section form is NACA4420 with the chord length of 0.3 D_p.

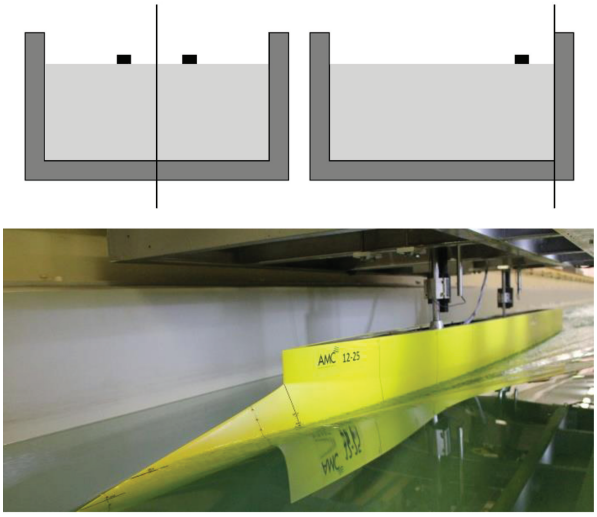

Figure 5 Top: Concept of a single catamaran demihull towed in close proximity to the tank wall for realising larger models and scale factors for catamarans. Bottom: A photograph of a 4.35 m long model of a high-speed wavepiercing catamaran demihull towed in th in the 100 m long AMC towing tank (Zurcher 2015)

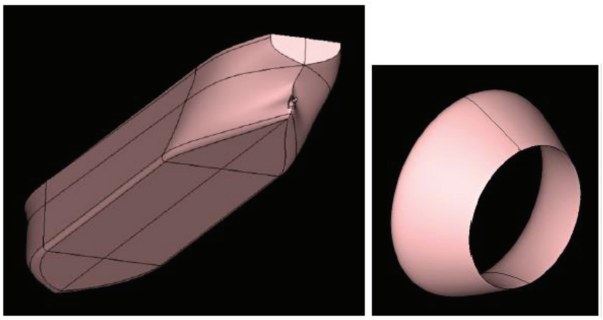

Figure 6 Geometries of a ship hull (left) and a duct(right)

Table 1 Principal particulars of a ship

L_{pp}[m]	Lwl[m]	B[m]	D[m]	d[m]	CB
280.0	285.0	45.0	25.0	16.5	0.858

Table 2 Principal particulars of a propeller

Dp[m]	H/D	BR	AR	No. of blades	Blade section
8.12	0.75	0.18	0.50	5	AU

The ship model with the scale ratio of 1/40 (i.e. L_{pp}=7.0m) was constructed and tested in the 400m towing tank of the National Maritime Research Institute. Also, the flow field measurement was carried out using the SPIV (Stereo Particle Image Velocimetry) system. Note thet the ship model is not equipped with a rudder, since a rudder may interfere with the leaser sheet of the SPIV. In addition, SPIV measurement using 3.2 m model is also conducted in Osaka University. The stern shape of 7m model with the duct and propeller is shown in Figure 7 Duct and propeller.

Figure 7 Duct and propeller

The Committee added this new benchmark data to the procedure 7.5-03-02-02: CFD, Resistance and Flow Benchmark Database for CFD Validations for Resistance and Propulsion.

2.3 Practical Applications of CFD

CFD can be a reliable tool to determine the drag of marine surface craft, as the relevant flow phenomena are resolved. However, in comparison to model scale experiments 3% – 8% of deviation in drag may still occur (Akbarzadeha et al. (2015), Kleinsorge et al., (2016), Ozdemir et al., (2014), Sun et al.

(2016).

For unconventional craft including multihulls and planing vessel, a certain deviation from experimental results may be expected. Jiang et al. (2016) used CFD to investigate a planing trimaran up to speeds of $Fr_V = 5.9$ for which the drag was under-predicted by 15%. However for speeds below $Fr_V < 5$, the drag was within 6% of the experimental measurements which is in the range of what De Luca et al. (2016) found who concluded with 5% − 8% under-prediction for a planing boat at Fr = 0.8-1.4. Eslamdoost (2014) predicted the drag within 4% for Fr = 0.2-1.6 for a 2.3 m planing monohull (Figure 8). Also at lower speeds (Fr = 0.2-0.45) under-prediction of 2% − 8% can occur for a 4.3 m high-speed catamaran model and less than 4% under-prediction for a 2.5 m medium-speed catamaran model (Haase et al. 2016b).

Numerical Full-scale Predictions and Its Validation Computational fluid dynamics can be used to directly determine the drag of the full scale ship, but it is difficult to validate these results due to the absence of controlled-environment testing facilities for full-scale ships. One approach is to simulate the self-propelled model and then compare to sea-trial results, which implies that not only the resistance is accurately predicted, but also the propeller performance and the propeller-hull interaction.

Ponkratov & Zegos (2015) modelled a steadily sailing ship (CB = 0.8) at design draught including the propeller and the superstructure using CFD and compared it to sea trial data at the same conditions. Shaft power was over-predicted by no more than 3% at $Fr = 0.19$. Extrapolated model test results were within 4% of the measured data. Simulations at model scale concluded with deviation to measurements no more than 3% for drag and propeller characteristics. They conclude that the ship-hull interaction may have been more accurately predicted in CFD, however, they also admit that it is difficult to support such a statement.

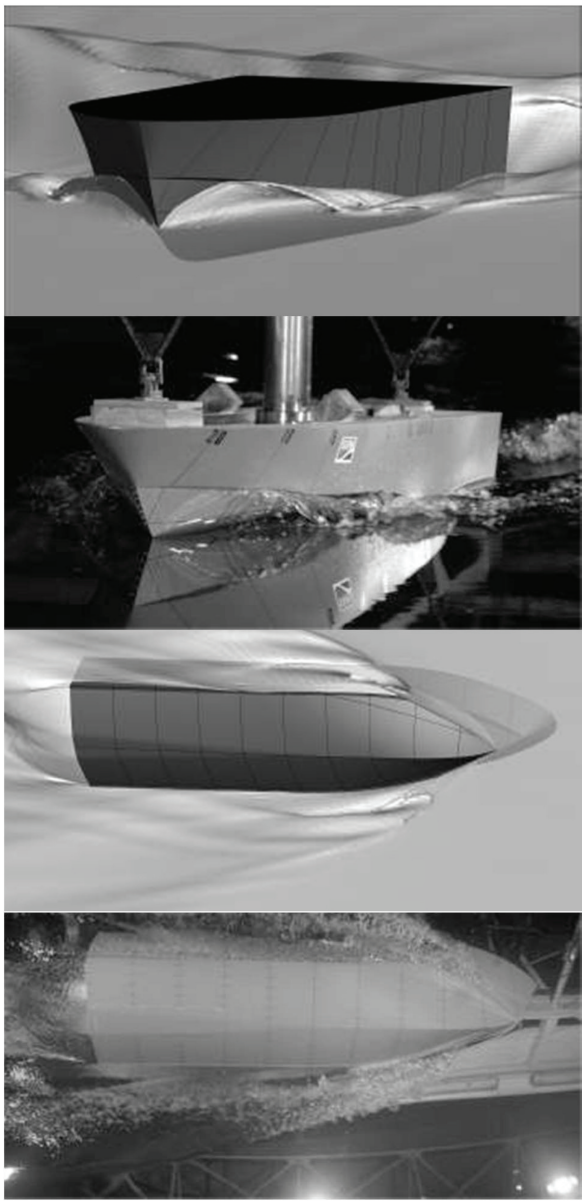

Figure 8 Free-surface from CFD and experiments from Eslamdoost (2014)

Mikkelsen & Steffensen (2016) also used CFD to predict the powering requirements for a 62,000 dwt bulk carrier (L = 200 m) at 14.5 kn. Compared to sea trials, CFD over-predicted the delivered power by 2%, while extrapolated model test data over-predicted by 6%. However, compared to the sea-trialled ship, a stock propeller was used and drag due to the superstructure, bilge keels and hull roughness was in included using empirical corrections from ITTC

guidelines instead of resolving the effects using CFD.

Haase et al. (2016b) used CFD to predict the full-scale drag in conjunction with model-scale experiments. They first modelled the ship (a 98 m high-speed wave-piercing catamaran) at model scale and after acceptable agreement with experimental data was achieved they simulated the vessel at full-scale Reynolds numbers. Instead of increasing the size and speed of the ship, they decreased the viscosity so that Froude and Reynolds number correlate to the full scale ship. The drag can then be linearly scaled to full-scale by form factor cubed (λ^3) and the ratio of fluid density (ρ_{SW}/ρ_{FW}), as outlined in Figure 9. While hull roughness was resolved, air drag was empirically considered. For Froude numbers around 0.4, sea-trial results were within the range of numerical predictions and extrapolated model scale data. At lower Froude numbers the model-scale data and CFD prediction under-predicted the sea-trial results. For estimating drag from the sea-trial results, they correlated shaft power with the thrust curves of the water jet propulsor and assumed that drag equals thrust.

CFD can be useful for predicting resistance components. Kinaci et al. (2015) simulated the KCS in single-phase double body simulations and multi-phase simulations, where the difference in drag can be attributed to the wave-making resistance. Park (2015) used CFD to investigate the form factor for the KVLCC2 and DTMB 5415 using the double-body approach. He subdivided the form factor into frictional and viscous pressure components. The contribution due to the viscous pressure loss was more than twice as significant when compared to the additional friction. For both models the increase in friction was comparable, but the pressure losses for the KVLCC2 were twice as big when compared to the DTMB model. For Reynolds numbers of 1×10^7-3×10^8 the form factor increased by up to 10% when using ITTC ship-model correlation line, while it

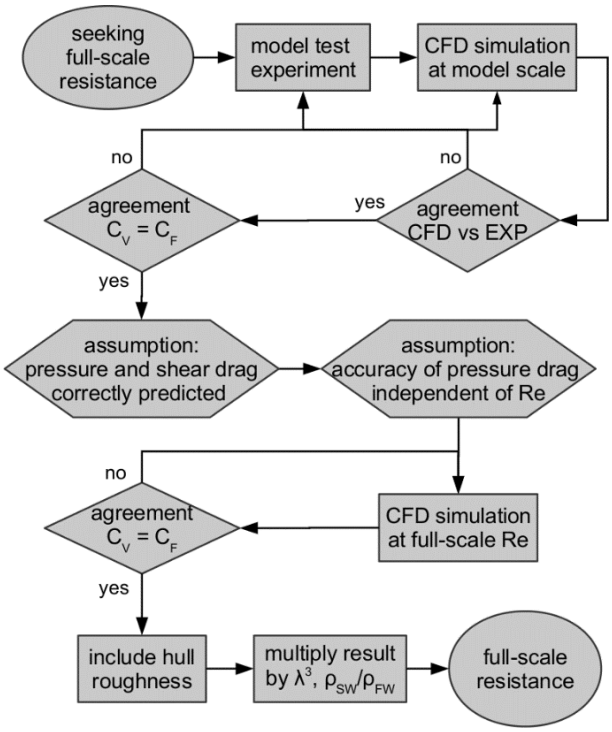

Figure 9 Flow chart for using CFD to predict the full-scale drag in conjunction with model-scale experiments (Haase et al. 2016b)

only increased by less than 4% when using the Grigson line instead. Also Wang et al. (2016) investigated the form factor as a ratio of pressure drag over frictional drag for a double-body tanker. Their results concluded that the form factor is 3% smaller for the full-scale ship when compared to model scale.

For industrial applications, turn-around times, when using CFD in the simulation-based design process, can be reduced if integrated software approaches are used (Stern et al. 2015, Kleinsorge et al. 2016).

Despite the advances using viscous CFD, there are still many developments for potential flow solver. These are mainly used for investigating wave-making drag with much shorter turn-around times and hence are suitable for large design space exploration and model comparison in the early design stage of a vessel. Deviations of 10% may be expected. Examples

include: Peng et al. (2014), Yang et al. (2016), Chen et al. (2016), Yua et al. (2015), Ginnis et al. (2013), Will & Koempe (2015), and Tsubogo (2016).

Sherbaz & Duan (2014) and Sun et al. (2016) have used CFD for establishing the effect of trim angle on the calm water resistance for reducing fuel consumption during operation. They both concluded with a trim towards stern for reducing drag. Sun et al. (2016) found very close agreement between his extrapolated CFD results (using ITTC' 57 approach) and sea-trial measurements at different trim angles.

The effect of Reynolds number (scale effect) on the form factor has been investigated by RANS equations-based CFD analysis in (Kinaci et al., 2016). It was found that the form factor depends on Reynolds number almost linearly. This means that once two form factors are computed (or measured experimentally) at very low Froude numbers, one can easily apply linear extrapolation technique to get the full scale Reynolds number form factor.

Extrapolation/Scaling Hagesteijn et al. (2016) note the large scatter of correlation values when deriving the powering requirements at design draught based on sea-trial data at ballast conditions. A low value suggests low drag and thus low fuel consumption. A low value is desirable for the ship operator, but if the value is too low, the service speed could be underestimated and the propeller overloaded which leads to more cavitation, noise, erosion, and potentially to shorter docking intervals. They highlight the role of CFD for understanding and predicting scale effects which then could lead to lower correlation allowance values and more accurate powering prediction.

For vessels with a deep transom stern, the drag coefficient is highest when the transom runs dry (Eslamdoost et al., 2013). Haase et al. (2016c) found that the transom can contribute up to 70% of the total drag for the full-scale vessel and that the dry-state at full-scale occurs at lower Froude numbers (dFR=0.02). The authors highlight that CFD is capable of accurately predicting this effect (Figure 10) and consider it as a non-linear scaling effect that is taken into account when using CFD for extrapolating model test results.

Haase et al. (2015) studied the drag properties and attitude of a hull form family for large medium-speed catamarans (Fr = 0.25-0.49) at full-scale, using the approach presented in Haase et al. (2016b). The hull form study at full-scale Reynolds numbers is supposed to eliminate any scaling effects between the model and full scale predictions.

For submarines, often a non-skid coating is applied on the top side of the hull which exceeds typical hull roughness values (Shen & Hess, 2011). The increase in drag force is not primarily caused by an increase in shear force, but rather by eddies originating from the protrusions of individual roughness spikes. For scaling the boundary layer on such surfaces, Shen & Hess (2011) derived a momentum boundary layer thickness similarity method for roughness scaling which agreed well with results obtained from free-running submarine models. Correlation formula for predicting model-scale roughness to mimic non-skid surfaces:

$$h_m = h_s\left(\frac{1}{\lambda}\right)\left(\frac{Re_{xm}}{Re_{xs}}\right)^{-0.2} = h_s\left(\frac{1}{\lambda}\right)(\lambda)^{0.3}\left(\frac{V_m}{V_s}\right)^{0.2} \quad (1)$$

Shen et al. (2015) introduced a novel approach for extrapolating model-scale drag. For an axis-symmetric body, they divided the body into a laminar and a turbulent part. The model-scale form factor was calculated for the partly laminar-turbulent flow, while it was predicted for the full-scale body with fully or almost fully turbulent flow. This leads to different form factors at model and full-scale Reynolds numbers. When using tripping devices, the laminar

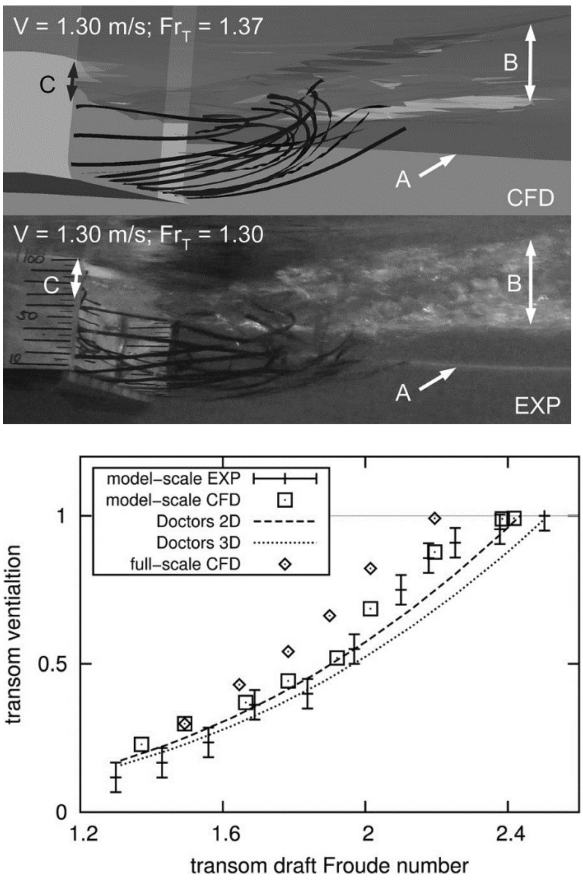

Figure 10 Upper: Flow pattern in the stagnant area past the partially ventilated transom of a high-speed catamaran by numerical prediction (top) and experiments (bottom). Lower: State of transom ventilation determined by experiments, empirical formulations, and CFD at model and full scale(Haase et al. 2016c)

area can be accurately predicted. The current ITTC'78 extrapolation procedure is considered a special case (where the form factor is independent of Reynolds number) of the presented approach.

Drag Prediction in Finite Water Patel & Premchand (2015) studied the DTMB 5415 at h/T = 1.5 at length Froude number (Fr) from 0.15 to 0.36 which correlates to depth Froude numbers (Frh) of 0.6-1.6. For depth Froude number of 1.0 and below, their results are with 7% of an empirical prediction by Karpov. The highest drag (270%), when compared to deep water, was found at Fr_h = 1.1.

Mucha et al. (2016) investigated the KCS, DTC and KVLCC2 in shallow water conditions (h/T = 1.2, 1.3) at model scale. At speeds below 1 m/s CFD and experiments showed good agreement in drag. At the highest speed tested, the deviation went up to 10% and 20% for at h/T = 1.3 and 1.2 respectively, for DTC and KCS. For the KVLCC2 good agreement over a range of speeds (0.2-0.7 m/s) was achieved. For predicting sinkage and trim, a Rankine-source panel method and a slender-body theory approach were also investigated. CFD lead to more accurate prediction, BEM and SB methods are acceptable at the lower speed range. Also, good results for the KCS at high speeds with the Rankine-source approach can be achieved (Gourlay et al., 2015). Generally, sinkage is more accurately predicted that trim.

Tezdogan et al. (2016) studied the DTC hull at depth Froude numbers (Frh) from 0.2-0.5, for Fr < 0.12. Compared to experiments, squat deviated by up to 10% which was within the experimental uncertainty. A critical depth Froude number between 0.4 and 0.5 was found, after which the resistance rapidly grew, especially due to an increase in friction at the hull.

Haase et al. (2016a) investigated a 2.5 m model of a 130 m medium-speed catamaran. Speeds of Fr=0.37, and 0.45 were investigated at different draughts relating to Frh=0.37-0.92. CFD predictions and experimental measurements within 6%. With CFD they predicted that for a tank width of b/L=1.4 a depth of h/L =0.7 is required to have residuary resistance deviating less than 1% from an infinitely deep tank. For a shallow water case (h/L=0.24) they found that the tank width needs to be at least b/L=3 at Fr=0.37 to have residuary resistance deviating less than 1% when compared to an infinitely wide tank and at b/L>15 for Fr = 0.45. Values for infinitely deep or wide tanks were achieved using Richardson extrapolation of finite tank dimensions. Furthermore, they

predicted the drag for full-scale catamarans. For a 98 m high-speed catamaran at 18 knots at h/L = 0.12-0.17, CFD under-predicted the drag by 17% – 32% while corrected model-test results would have underestimated drag by 33% – 40%. When comparing full-scale simulated drag of the 130 m catamaran with the extrapolated experimental results, a difference up to 11% was reported, whereas CFD predicted up to 12% less pressure drag than residuary resistance (determined by experiments) and up to 35% more viscous drag.

Gao et al. (2014) used CFD to investigate the drag of a KVLCC2 model advancing in shallow water (h/T = 1.2) where the sea floor is covered with mud, from 0.0 to 0.4×T above the sea bed, meaning that the lower 20% of the vessel hull was covered in mud. The mud was modelled as a Bingham plastic with a density of 1220 kg/m^3. Results suggest that the ship's penetration into the mud should be less than 10% of the ship's draught to avoid excessive drag. The increase in drag is mainly addressed to an increase in shear stress where the mud covers the hull.

Gao et al. (2015) numerically studied the drag of a Wigley hull when advancing in muddy waters using the Herschel-Bulkley model for simulating the mud (Figure 11). Similar to the above study, the frictional drag increases once the ship starts penetrating the mud.

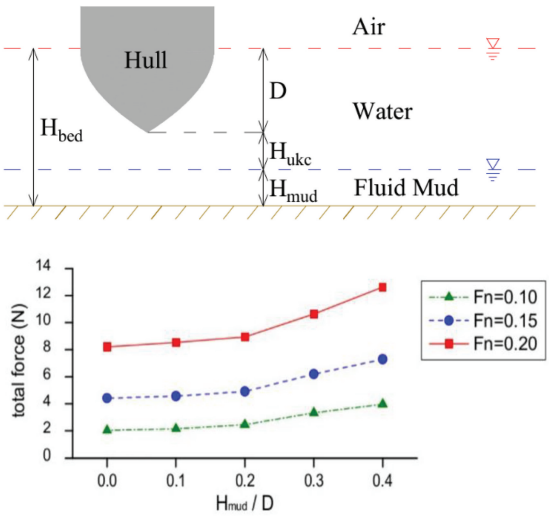

Figure 11 Top: Three phase (air, water, and mud) for a hull advancing in shallow water with muddy ground. Bottom: Drastic increase in drag once the hull penetrates the mud for $H_{mud}/D>0.1$ (Gao et al. 2014)

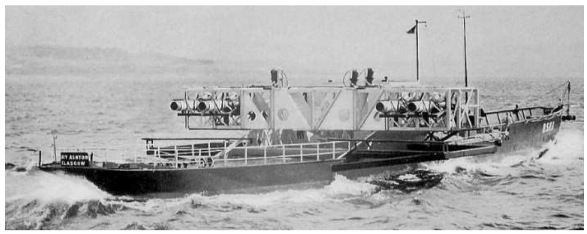

Figure 12 The Lucy Ashton, a former paddle wheeler with jet turbines for measuring full-scale drag
(flickr. com/photos/scottishmaritimemuseum/)

2.4 Need for Research and Development

The need for research and development for improving methods of full-scale powering predictions.

One popular attempt was made to validate full-scale drag predictions (Denny & Maurice 1951), where the paddle wheeler *Lucy Ashton* (see Figure 12) was powered with air borne jet turbines on a force balance to avoid any hull-propulsor interaction. However, a considerable effort was required.

Ponkratov & Zegos (2015) stated that in sea trials the propeller torque, shaft rpm and speed can be sufficiently accurately measured for CFD validation purposes. However, propeller thrust is difficult to obtain, because the longitudinal deformation of the shaft is in the same order of magnitude as the equipment tolerances.

Mikkelsen & Steffensen (2016) claim repeatability of full-scale powering measurements

between four sister ships. However, when comparing sea trial powering measurement with measurements of ships in service, they found an increase in power requirement of 8%, which was related to bio-fouling effects. They state that sea trials are a "trustworthy reference" for extrapolated towing tank data and full-scale CFD predictions. They furthermore state the issue that most sea trials are conducted at ballast conditions, even though it is an off-design case.

Ponkratov (2016) provided sea trial measurements of a cargo ship in ballast conditions. The ballast draught may have led to a low aft draught and resulted in a relatively low propeller immersion and thus negatively impacted the uncertainty of the measured data.

Full-scale powering predictions using CFD appear to have the potential for being practically applicable and can be validated by measurement in sea trials. However, the above cases have the drawback of representing a hull largely unaffected by bio-fouling or sailing at ballast draught, which both is not applicable to the typical ship in operation.

3 PROCEDURES

3.1 Requirements for Changes

The committee determined that the following procedures would benefit from updating:

- 7.5-01-01-01 Ship Models—Revised sections on construction materials, surface finish, manufacturing tolerance, turbulence stimulation and updated references.
- 7.5-01-03-04 Benchmark for PIV(2C) and SPIV(3C) setups
- 7.5-02-02-01 Resistance Test—Revised definition of variables to include new variables that were missing, sinkage and trim, corrected oscillation period formula, added section on extrapolation to full scale, updated uncertainty analysis and updated references.
- 7.5-02-05-01 High Speed Marine Vehicle Resistance Test—added missing variables, added information on sand strips, speed measurement instrumentation, thermometers, data acquisition methods, data reduction and updated references.
- 7.5-03-01-01 Uncertainty Analysis in CFD Verification and Validation Methodology and Procedures—a minor update of Revision 02, in which the references to the ISO document have been updated to the latest issue of the JCGM GUM, and further details of the Least Squares Root method for estimating error have been added.
- 7.5-03-01-02 Uncertainty Analysis in CFD, Guidelines for RANS Codes—minor editorial revisions.
- 7.5-03-02-01 Uncertainty Analysis in CFD Examples for Resistance and Flow—minor editorial revisions and corrections.
- 7.5-03-02-02 Benchmark Database for CFD Validation for Resistance and Propulsion—updated to include reference the 28th ITTC RC report discussion of benchmark database.

The following procedures were determined by the RC and AC to not require an update:

- 7.5-02-01-01 Guide to the Expression of Uncertainty in Experimental Hydrodynamics
- 7.5-02-01-03 Fresh Water and Seawater Properties
- 7.5-02-02-02 General Guidelines for Uncertainty Analysis in Resistance Tests

- 7.5-02-02-02.1 Example for Uncertainty Analysis of Resistance Tests in Towing Tanks
- 7.5-02-02-02.2 Practical Guide for Uncertainty Analysis of Resistance Measurements in Routine Tests
- 7.5-02-04-02.1 Resistance Test in Level Ice
- 7.5-02-04-02.5 Experimental Uncertainty Analysis for Ship Resistance in Ice Tank Testing
- 7.5-03-01-01 Uncertainty Analysis in CFD, Verification and Validation Methodology and Procedures
- 7.5-03-01-02 Uncertainty Analysis in CFD Guidelines for RANS Codes
- 7.5-03-02-01 Uncertainty Analysis in CFD Examples for Resistance and Flow
- 7.5-03-02-03 Practical Guidelines for Ship CFD Applications
- 7.5-03-02-04 Practical Guidelines for Ship Resistance CFD

3.2 Need for New Procedures

The RC had a number of discussions on possible new procedures and guidelines. While there are a number of new and innovative experimental techniques, numerical models, and model construction methods, the RC felt that all of these areas are too premature to warrant the need for ITTC procedures, and that the current procedures provide adequate guidance at this time. Future committees should continue monitoring these advances and develop the necessary guidelines/procedures as these areas become more established.

4 SHIP SURFACE ROUGHNESS

When performing experiments on scale models of ships the hulls are considered hydraulically smooth, whereas full-scale ship hulls are subject to paint, marine growth (ranging from soft slime to hard barnacles) and geometric imperfections, including dents, paint defects, weld lines, and plate thickness differences. These impact the drag force and the flow into the propeller (Guiard et al., 2013, Lindholdt et al., 2015). Relative to the fully turbulent flow over a smooth plate, the skin friction coefficient for flow over a rough surface increases with increasing Reynolds numbers. However, in absolute terms the skin friction coefficient for rough surfaces is independent of Reynolds number once being in the fully rough regime, as shown in Figure 13.

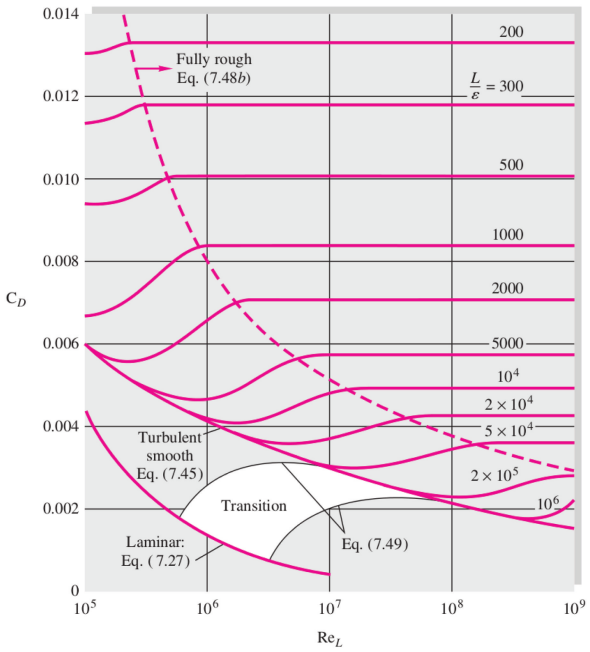

Figure 13 Drag coefficient for a flat plate of different roughness at a range of Reynolds numbers (White, 2009)

Measurements by Ponkratov (2016) suggest that the hull roughness of an operating, but freshly cleaned 138 m cargo vessel varies from

70-270 μm depending on the position on the hull.

The exact roughness of the hull is mostly unknown. Consequently, Haase et al. (2016b) investigated a hull with equivalent sand grain roughness of 100 and 200 μm and concluded with reference to ITTC guidelines (which suggested 150 μm if the exact value is unknown) that the exact value should be in between these two. Full-scale measurements for a 98 m high-speed catamaran were within the predicted range for Fr around 0.4.

Shen & Hess (2011) found that for very rough surfaces, such as non-skid surfaces on submarines, the increase in drag is dominated by additional eddy drag induced by the roughness elements, rather than by the increase in skin friction drag. Thus they proposed a momentum boundary layer thickness approach for considering an appropriate roughness in model-scale experiments.

Bio-fouling From comparison of sea-trial results and powering data of the same vessel in service, Mikkelsen & Steffensen (2016) concluded that marine growth caused additional drag of 8%.

Walker et al. (2014) and Schultz et al. (2015) measured skin friction drag of coated and fouling-affected plates with purposely cultured biofilms. Using a scaling approach of Granville, Walker et al. (2014) concluded for friction increase up to 3% for AF (anti-fouling) coating (less than 1% for fouling release coating) when compared to a smooth surface on 150 m ship at 30 knots. However, for a vessel covered in moderate slime film, friction increased by 48% leading to 19% increase in total drag.

Monty et al. (2016) measured the drag of a tubeworm covered plate in a wind tunnel and concluded an equivalent sand grain roughness of 325 μm. This leads to an increase in friction by up to 59% and the total drag up to 34% considering a frigate and VLCC at different speeds, if residuary resistance was unaffected.

Turan et al. (2016) towed a smooth plate with 5% – 20% coverage of artificial barnacles for investigating the impact on the drag. They concluded that friction on a LNG carrier increases by up to 37% – 98% and drag by 23% – 60% for the 5% – 20% barnacle coverage if residuary resistance was assumed being constant.

Demirel et al. (2014) and Vargas & Shan (2016) validated different CFD models in a towing tanks using surface piercing rough flat plates covered with different AF coatings. They both found that the CFD model was capable of predicting the drag within 2% – 2.5% of the measured values.

Demirel at al. (2016) have further applied their CFD model to investigate the increase in effective power at the full-scale KCS for two speeds (19, 24 knots) for a variation of roughness ranging from smooth, to that of AF coatings, of slime, and of heavy calcareous fouling. Compared to Monty et al. (2016) and Turan et al. (2016), they also investigated the effect on residuary and wave-making resistance. With reference to the smooth hull, the coating increased the friction up to 11% and the powering requirement up to 7% and in the heavy calcareous case these figures reached 170% and 130% respectively. The wave-making drag for the AF coated hull reduced by 5% when compared to the smooth case, which was even more pronounced for the heavy fouling case where it reduced by 72%. The relative reduction in wave-making was more pronounced at 19 knots when compared to the 24 knot case. Nevertheless, the reduced wave-making drag occurred at the cost of a higher total drag force. The wave patterns for a smooth and heavily fouled hull are shown in Figure 14.

Lindholdt et al. (2015) have conducted a comprehensive review on bio-fouling and relat-

ed drag penalties for ocean-going vessels. They concluded that small scale tests for hull coatings are important and common, but more insight on fouling species, mechanical roughness, and aging effects of the hull was missing. They proposed that more research on the applicability of small-scale testing for full-scale applications is required. Also, they suggest a replication of the ships operating pattern (static and dynamic) when considering drag performance investigations. While surface roughness can be described with only one parameter (e.g. equivalent sand grain roughness), the density and shape of the roughness elements should be taken into consideration. However, they mention even when including more parameters on the roughness and its distribution, accurate prediction are still difficult to achieve. Generally, drag penalties due to hard macro-fouling is better understood than losses due to soft bio-fouling. Different types of fouling are shown in Figure 15.

Ice Interaction For accurately modelling the friction between a ship and sea ice, Cho et al (2015) investigated different materials and paintings to achieve a desired friction behaviour in model-scale experiments. They concluded that the addition of small amounts of MgSi to lacquer and diluent was desirable. With this method, the frictional coefficient between a test sample and fresh water ice could be controlled in the range of the target value.

Superhydrophobic Surface Superhydrophobic coatings and surfaces are becoming an increasingly popular technique for the reduction of drag in applications involving the flow of liquids over solid surfaces, for a wide range of Reynolds number, from laminar to turbulent conditions. Such coatings work by the interposition of a gas layer between the liquid and the solid wall, trapped by distributed microscopic roughness elements present at the wall. Liquid can flow over the gas layer with negligible friction.

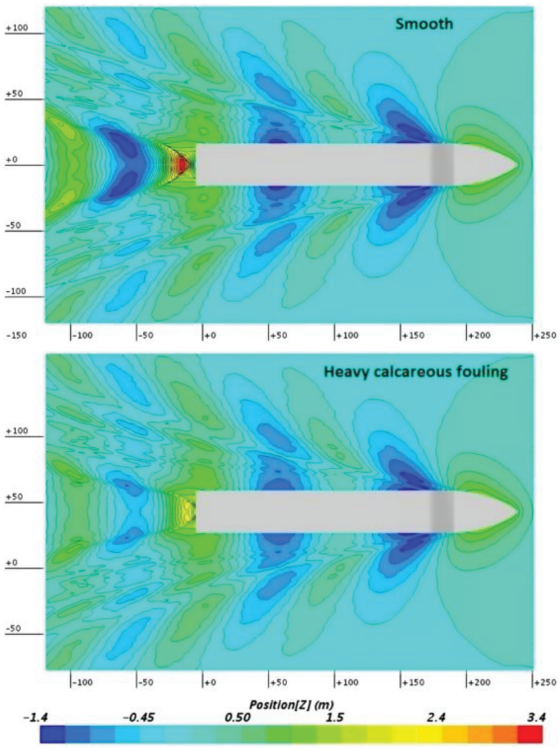

Figure 14 Wave making of the KCS at 24 knots for a smooth hull (top) and a hull affected by heavy calcareous fouling (bottom) (Demirel et al, 2017)

Dr. Anish Tetuja, Assistant Professor of Materials Science and Engineering at the University of Michigan, Ann Arbor, recently published two articles that have garnered significant popular press coverage. In the work, "*Hygro-responsive membranes for effective oil-water separation*" (Arun et al., 2012) they developed the first-ever solely gravity driven methodologies for the separation of a range of different oil-water mixtures. Listed below are links to some of the popular press coverage. Overall well over 100 newspapers, magazines and websites have highlighted this work.

Dr. Tetuja's group also developed one of the first ever surfaces on which any liquid, including various oils, alcohols, blood, acids and bases, bounce and roll-off. Their paper entitled, "Superomniphobic Surfaces for Effective Chemical Shielding" (Pan et al., 2013) has been highlighted by over 100 publications.

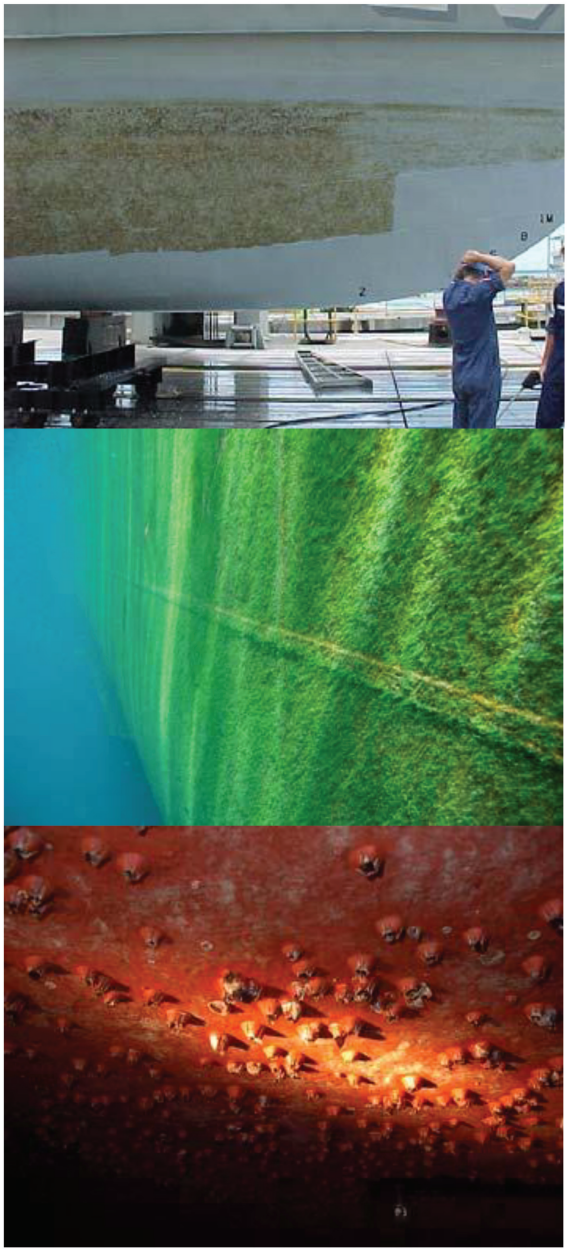

Figure 15 Different types of bio-fouling: Slime (top), weed (middle), and barnacles (bottom) (Willsher, 2007)

5 WAVE PROFILE MEASUREMENTS METHODS

Typical towing tank methods for measuring steady (constant ship speed) ship generated waves have included marking the steady wave profile contact line with a grease pencil and the post run measuring the change from the design waterline, using resistive wave staff, and finger probes. Very few organizations routinely make wave profile measurements. At one time it was not uncommon for the steady ship generated transverse wave field to be characterized to estimate the wave resistance. The improved ability of CFD to be able to accurately estimate wave, viscous, and total resistance has led to the scarcity of this type of towing tank work. When the RC polled the members on which institutions had documented procedures for wave profile measurement only two organizations still made these types of measurements. When these procedures were reviewed it became clear that these techniques were being used not to charcterize wave resistance, but to validate CFD codes. They were also focused on unique applications and experiments. Since so little steady wave resistance work was taking place and that there was no well established organizational techniques or testing, ITTC guidelines and procedures were not warranted.

There is work being done that may be relevant in the future to the ITTC. Work in measuring turbulent free-surface flows (wave breaking), typically optical, laser based methods have been developed. The break-up of a turbulent liquid into spray is a complicated multiphase flow problem with complex break-up mechanisms. Currently, direct simulation of these processes is impractical due to the large range of scales and the requirements on grid resolution and computation time. Because of these limitations, experimental studies have been used to develop semi-empirical closure models and these have relied on advance measurement techniques. Experimental research on liquid sheet break-up has been performed to improve the understanding of free-surface break-up mechanisms (Fu et al., 2012 and Hackett et al., 2012). While circular liquid jets have been studied extensively, e.g. Lin & Reitz (1998), geometrical and scale differences make the break-up of a liquid sheet different from both circular free and wall jets, although the

mechanisms leading to the sheet's break-up can be similar (Dai et al, 1998). These structures cause the liquid surface to roughen, and create ligaments, which results in spray production. As examined by Sarpkaya and Merrill (2000), ligaments elongate until surface tension effects result in the tip pinching off of a ligament to create a droplet.

A number of quantitative visualization techniques have been utilized in experiments focused on the break-up of a turbulent liquid wall jets and breaking waves. Shakeri et al. (2009) utilizes a cinematic laser-induced fluorescence (LIF) technique to meausure breaking wave profiles. The features of the breaking process can be easily identified. The focus of these types of efforts are to investigate mechanisms and provide data for assessment of numerical simulations of the bulk properties of the fluid and resulting spray.

6 ROUGHNESS OF MODELS AND APPENDAGES

The Final Report of the 27th RC provides an overview of the various rapid prototyping techniques in common use, such as: stereo lithography; laser sintering; inkjet/3D printing; masking process; fused deposition; and laminated object manufacturing. A review of published literature on the subject identified a huge number of publications on rapid prototyping in general, on all facets of the process and a broad range of applications, and many note that the surface roughness of parts manufactured is critical as this can affect part accuracy, reduce the post-processing finishing costs and improve functionality of the parts. However, no publications could be identified that specifically deal with the manufacture of hydrodynamic/ship models or appendages and the effect that their surface roughness has on resistance measurement.

Bennett et al. (2015) performed an initial investigation into the use of 3D printing technology to manufacture a structurally accurate flexible towing tank model for assessing the consequences of wave-ship interaction from a ship structural design perspective. The material properties of different 3D printed materials were assessed for their ability to model the scaled structural behaviour of a ship. Practical considerations for the construction of 3D printed models were discussed, including the constraints imposed by the limited size of printer beds for currently available units, thus requiring a modular approach for constructing large ship models.

Adelnia et al. (2006) conducted a study to determine the suitability of models constructed using rapid prototyping methods for use in subsonic and transonic wind tunnel testing by comparing against more conventional models constructed of aluminium. In general, good agreement was found, except for runs involving higher loading where it was assumed that the 3D printed models were bending. The authors also noted that the surface finish of the 3D printed models was not as smooth as the aluminium model and that this had a measurable effect on the aerodynamic characteristics.

A benchmark study that quantified and compared mechanical and other properties of parts produced by various rapid prototyping processes was performed by Kim and Oh (2007). This included tensile, compressive and impact strengths, hardness, heat resistance, dimensional accuracy, manufacturing speed, material costs and surface roughness. It was found for all methods that the tensile and impact strengths were strongly dependent on the build direction, and as the surface inclination increases, in most cases, the surface roughness decreases owing to the reduction of "stair stepping" (a dimensional shift as each layer is printed). It was noted that the findings are somewhat dependent on factors such as experience of operators, environmental conditions and states of the materials used. Another

benchmark study was performed by Mahesh *et al*. (2004) in which a purposely-designed part was designed and fabricated to evaluate many of the abovementioned mechanical properties and features, but interestingly did not appear to include surface finish.

In order to inform the ITTC community of the surface roughness of typical ship models and items produced using rapid prototyping techniques (3D printers) the 28th ITTC RC have quantified the surface roughness of existing ship models manufactured from a range of 'traditional' materials and manufacturing techniques and compared these to test samples produced using rapid prototyping methods (for various materials and machine-specific settings). This study has also assessed how this surface roughness affects frictional resistance.

Finally, discussion has been included on some of the known practical issues that have arisen with the use of rapid prototyping/3D printers for producing ship models and appendages. The focus of the study is on additive technologies, whereby the object is created by adding layer by layer of a liquid, powder or sheet material to produce plastic, ceramic, metal or composite parts (traditional "subtractive" methods such as CNC machining have been ignored).

6.1 Surface Roughness Comparison

The surface roughness of several existing ship models and typical raw test samples produced by different 3D printers was quantified using a commercially available surface roughness meter using a stylus-based direct measurement, refer Figure 16[Mitutoyo model 178-561-02E, typical cost around US $ 2,000 (Mitutoyo, 2017)]. The surface roughness was evaluated by the ISO 4287: 1997 method (ISO, 1997), which defines the following parameters for use as indices of surface roughness evaluation:

- Ra (μm): Arithmetic mean surface roughness
- Rz (μm): Maximum surface roughness
- RSm (μm): Significant period of surface roughness

The first two parameters, Ra and Rz, are focused on the *height* of the roughness (as defined in Figure 17), while RSm considers the *period* of the roughness (defined in Figure 18). It is the roughness height that is considered to be the index that most affects ship model resistance. Applying a Fast Fourier Transformation (FFT) to the measured surface profiles, significant period λ (μm) and maximum amplitude h (μm) of each profile were also determined. By comparing the two, the roughness characteristics of each ship model and test sample can be clarified.

Figure 16 Stylus type surface roughness meter

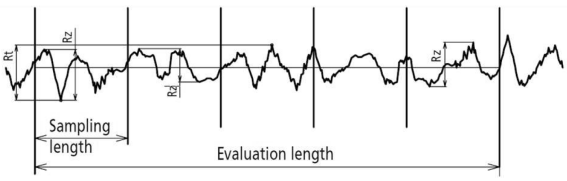

Figure 17 Definition of maximum surface roughness Rz from ISO 4287:1997

The selected ship models covered a range of traditional materials including paraffin wax, polyurethane foam (with lacquer) and wood (with lacquer) which were constructed to meet the commonly accepted standard for ship mod-

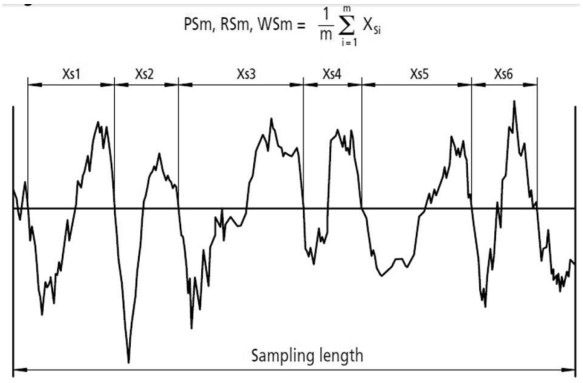

Figure 18 Definition of significant period of surface roughness RSm from ISO 4287: 1997

els provided in ITTC Procedure 7.5-01-01-01 (which is equivalent to that achieved with sanding using 300 to 400 grit wet and dry paper). For comparative purposes, the surface roughness of a polished metal propeller was also included. The results are provided in Table 3.

Table 3 Surface roughness measurements and particulars of ship models

Material	Paraffin Wax	Polyurethane (lacquer coating)	Metal
Model Type	Tanker	Patrol vessel	Propeller
Ra (μm)	1.1	0.3	0.1
Rz (μm)	2.7	2.1	0.8
Lwl (m)	8.0	5.0	
Vm (m/s)	1.30	3.50	
Re ($\times 10^7$)	1.04	1.75	
Rz/Lwl	0.38	0.42	

Similarly, measurements were made to quantify the surface roughness from a number of raw test samples produced by two different rapid prototyping 3D printers (“FlashForge Creator Pro” and “Catalyst Ex”), covering a range of manufacturing process variables such as: material, print speed and print orientation. Each sample consisted of a 30 mm×30 mm×5 mm thick flat disc.

The measurement results for eight individual samples made with “FlashForge Creator Pro” are shown in Table 4. The surface profiles of the samples displaying the maximum (Sample “a”) and the minimum Rz value (Sample “d”) are compared in Figure 19. The results of the FFT analysis on these two profiles are shown in Figure 20. Similarly, the measurement results from twelve samples made using the “Catalyst Ex” 3D printers are shown in Table 5 and Figure 21 and Figure 22 (for Samples “D” and “I”).

Table 4 Surface roughness results-FlashForge Creator Pro 3D printed samples

ID	ISO			FFT	
	Ra (μm)	Rz (μm)	RSm (μm)	h (μm)	λ (μm)
a	13.4	87.7	973.4	13.1	595.0
b	8.6	50.3	1035.5	7.4	1135.9
c	15.4	68.7	1291.2	13.5	2082.5
d	2.9	14.2	906.1	2.0	1249.5
e	7.9	36.5	987.6	8.8	1135.9
f	10.4	53.9	873.2	10.0	568.0
g	13.3	68.6	1161.9	10.7	1249.5
h	7.2	28.7	962.1	5.9	1249.5

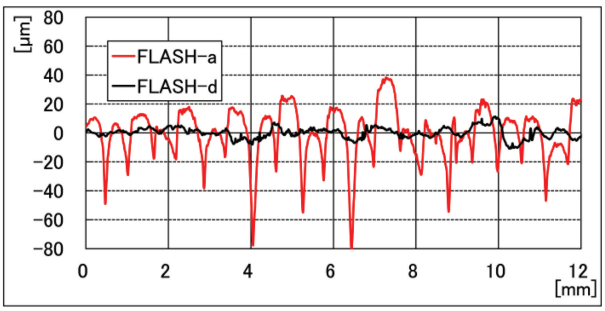

Figure 19 Comparison of surface profile for two FlashForge Creator Pro 3D printed samples

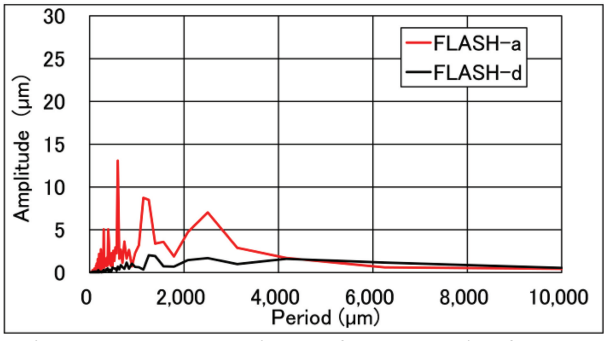

Figure 20 Comparison of FFT results for two FlashForge Creator Pro 3D printed samples

Table 5 Surface roughness results-Catalyst Ex 3D printed samples

ID	ISO			FFT	
	Ra (μm)	Rz (μm)	RSm (μm)	h (μm)	λ (μm)
A	9.2	45.2	545.3	7.0	1135.9
B	7.9	41.1	547.2	8.1	543.3
C	9.7	52.2	642.0	7.5	1135.9
D	27.0	130.0	550.1	25.5	1388.3
E	8.9	50.5	595.2	8.1	543.3
F	7.9	48.8	594.2	6.0	543.3
G	8.9	41.6	535.9	9.9	543.3
H	9.0	49.0	771.2	7.3	543.3
I	7.6	44.5	547.1	6.7	543.3
J	19.5	89.2	313.1	21.5	260.3
K	18.8	87.2	270.8	20.9	265.9
L	18.8	91.6	276.5	22.7	260.3

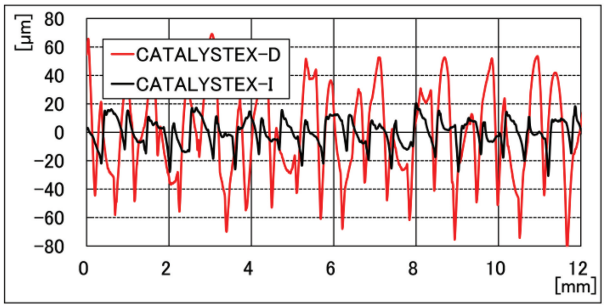

Figure 21 Comparison of surface profile for two Catalyst Ex 3D printed samples

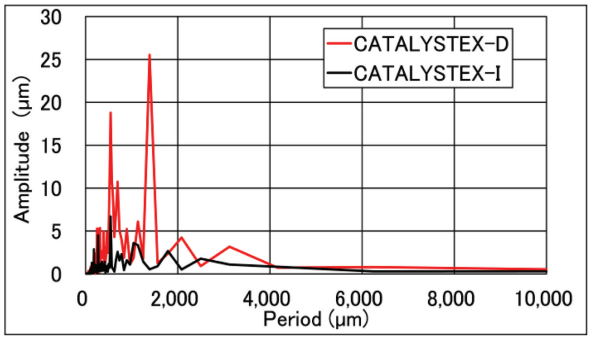

Figure 22 Comparison of FFT results for two Catalyst Ex 3D printed samples

In order to compare the roughness evaluation results from the two methods, the correlation between the ISO method and FFT analysis are shown in Figure 23. Regarding the roughness height, both the arithmetic mean (Ra) and maximum surface roughness Rz from the ISO method show good agreement with the maximum amplitude (h) from FFT analysis. However, for the roughness period, the ISO defined significant period of surface roughness (RSm) and the significant period (λ) from FFT analysis do not match very well.

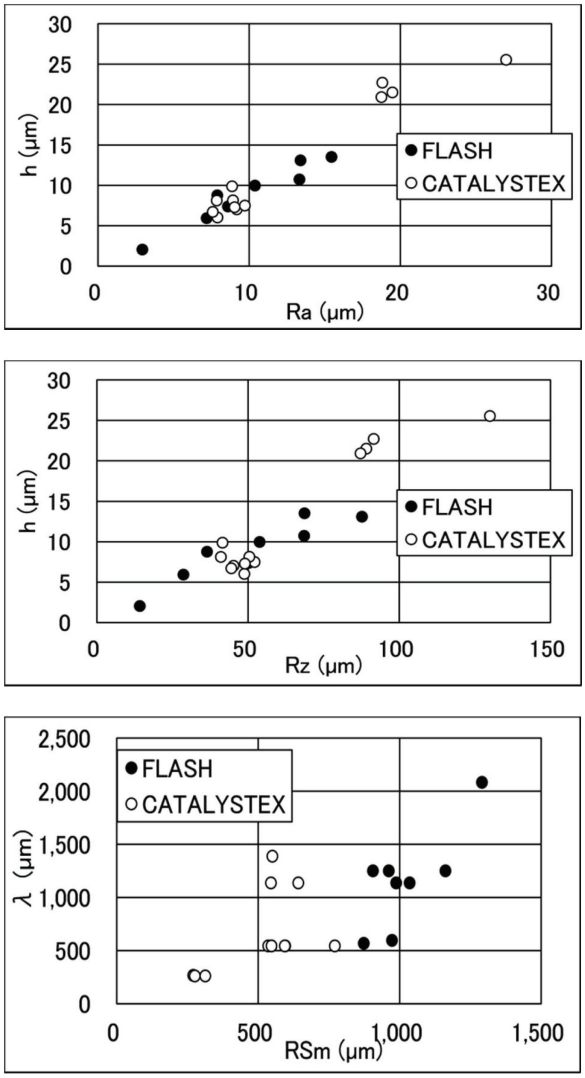

Figure 23 Correlation between ISO Roughness and FFT Results

The maximum surface roughness (Rz) defined in ISO 4287:1997 seems to better reflect the characteristics of the actual surface profile, compared to the maximum amplitude h (μm) obtained by FFT analysis.

Table 5, the raw surface finish of all rapid prototyping test samples, regardless of the material or method of manufacture, are considerably rougher than all of the ship models (Table 3). It is believed that the difference is too great, thus the raw finish from rapid prototyping is considered unacceptable for ship model resistance tests. Additional processes, such as sanding and sealing, is recommended prior to performing such model tests.

6.2 Effect of Surface Roughness on Resistance

To acquire accurate fluid force measurements it is necessary that the surface of the ship model during a towing tank test should be finished as smooth as possible and the influence of the surface roughness is eliminated. From this point of view, ITTC Recommended Procedures and Guidelines 7.5-01-01-01 on Ship Models (ITTC, 2011) recommend model surface finish as follows; "The model surface should be smooth and equivalent to that achieved with a 300 to 400 grit wet and dry paper", but there is no specific criteria of model surface roughness.

In order to consider the implementation of specific criteria for model surface roughness, a study was performed that employed the formula for the frictional resistance increment for sand roughness given by White (1991) to evaluate the influence on frictional resistance (see Equation 2).

$$\Delta u/U_\tau = \frac{1}{\kappa}\ln(1+0.3\cdot k^+) \qquad (2)$$

Where Δu is the non-dimensionalized velocity defect, κ is Karman's constant, and k^+ is non-dimensionalized roughness height.

Assuming that model surface roughness is equivalent to sand roughness, the frictional resistance increment due to roughness can be easily estimated. According to the empirical fact that the maximum roughness height Rz is the most significant value to determine the frictional resistance increment in case of an actual ship hull surface paint (Tanaka, 2003) the frictional resistance coefficient increased by roughness ΔC_F was obtained by substituting Rz in place of k^+ in Equation 1.

Examples of evaluation result of roughness influence to frictional resistance increment are shown in Figure 24, in which L is the length of flat plate. In this figure, roughness influence due to various roughness scale is expressed as the frictional resistance increment coefficient ΔC_F that is equivalent to "roughness allowance" for actual ship powering. When model ship length and its characteristic roughness height are known, the frictional resistance increment can be estimated easily using this kind of diagram.

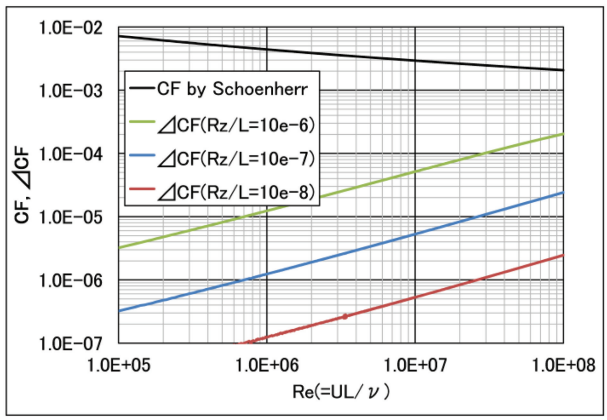

Figure 24 Evaluation results of frictional resistance increment for flat plate with various scale roughness

Furthermore, in order to clarify the influence on the resistance measurement in the towing tank test, the relative frictional resistance increment due to the model surface relative roughness Rz/L is shown in Figure 25. In this figure, the red hatched zone indicates model scale range of Reynolds number and approximate model scale relative roughness height range considering towing tank test speed and model length. When the size and roughness of

the model are specified, the influence on resistance increase due to surface roughness can be obtained. By comparing the resistance increment amount in the total resistance with the measurement accuracy or uncertainty or bias error inherent to each towing tank, it is possible to quantitatively evaluate the influence of the surface roughness of the model on the measurement result, and thus establish a criterion of satisfactory roughness for carrying out an accurate test. Therefore, by using the presented method, it is possible to easily investigate the influence on the measurement, not only for conventionally used materials like paraffin wax or polyurethane but also for new materials that may be adopted in rapid prototyping technology.

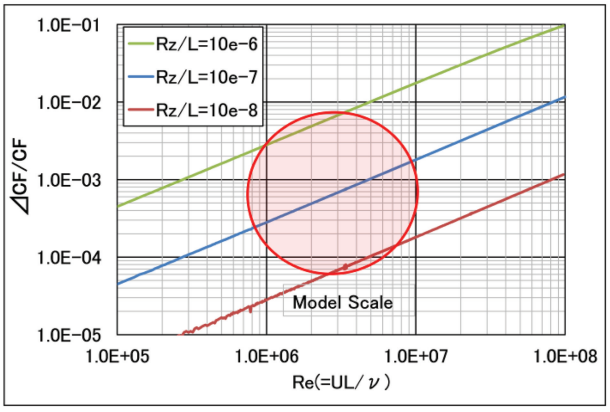

Figure 25 Relative Frictional Resistance Increment for Flat Plate with Various Scale Roughness

Table 5 for a range of ship model lengths from 2 to 8 metres. The results suggest that the effect that ship model surface roughness has on resistance is negligible (approximately 0.1% of C_F, 0.5% of C_T), provided that the model surface is finished according to the ITTC Recommended Procedure for ship models (7.5-01-01-01). However, in the case of the less than ideal raw surface finish from rapid prototyping techniques, the influence of the model surface roughness seems not to be negligible.

It is empirically known that the roughness effect is reduced when the roughness wavelength is sufficiently longer than the roughness height on the painted surface of actual ship hull (Sasajima, 1965; Mieno, 2012). Since this phenomenon is expected to occur on the model scale model as well, discussion of the results should be given careful consideration. Although the method considers only the wavelength, it is effective because it always gives a stricter standard.

Practical Issues Experienced with Rapid Prototyping

Most commercially available rapid prototyping units will provide the ability to change factors such as layer resolution, interior fill style, orientation, and support style. Changing layer resolution can affect surface finish and build times, for example, selecting a smaller layer resolution will usually create a smoother surface finish, but takes longer to build. The interior fill can affect the strength of the finished product. Generally, the options available include (a) solid, which produces a stronger, more durable part, but build time will be longer and more material is used; (b) sparse-high density, will reduce the build time and material usage, but with reduced strength, and (c) sparse-low density, with further reductions in strength, build time and material usage. Geometric distortion has been known to occur for all interior fill options, but found to be less likely for solid build. The orientation of the part to be printed can impact build speed, part strength, surface finish and material consumption. Often a part is stronger within a layer than it is across layers, so it is possible to orient a part to have its greatest strength across a specific area. In some techniques, there can be a significant difference in surface finish between horizontal and vertical orientation, with most attaining a better finish for a vertically oriented part than horizontal. For example, the print orientation for Samples "a" and "d" in Table 4 was horizontal and vertical respectively, and the significant difference is evident in Figure 20. It is common for

3D printers to incorporate different methods to support the item during the model build process to aid the build process and dimensional accuracy. The support material is removed when the part is complete.

The following list provides some facts and tips that may be useful when considering the use of rapid prototyping to manufacture ship models or appendages:

- Dimensional inaccuracies:
  - If items are long and thin they are likely to distort or warp.
  - The temperature during lay-up can impact print quality (and this can change with material selection).
  - Entry level printers can have low dimensional tolerance due to deformation of the part associated with internal stresses from thermal cooling resulting in a large variation in the structural properties between parts (refer Bennett et al. 2015 for more details).
  - The shell thickness can affect dimensional accuracy.
- Surface finish (orientation during lay-up): The tool path can influence surface finish (but often the software that drives the 3D printer provides little or no control over this).
- Stiffness: Materials such as nylon have been found unsuitable for models of propeller/rotors or other appendages that are required to remain rigid when under test conditions (Liu et al. 2015).
- Materials that absorb water or are porous need to be coated with a suitable sealant to eliminate/minimise water absorption.
- The surface of many materials have been known to become slimy when submerged in water for lengthy periods.
- Longevity: Further investigations into the long term effect of ageing on the performance of 3D printed materials in the marine environment are needed in order to develop a fully rounded understanding of the structural properties (Bennett et al. 2015).

7 UNCERTAINTY GUIDANCE

For reducing the uncertainty of towing tank measurements, Steen et al. (2016) found that when analysing towing tank data in multiple instead of single time windows, the uncertainty of the mean value can be reduced (see Figure 26). Furthermore, they have modelled the carriage and ship model as a moving mass-spring-damper system. Comparison of simulated and measured towing force allowed to conclude that the noise in the carriage speed is the main contributor for the noise in the resistance data.

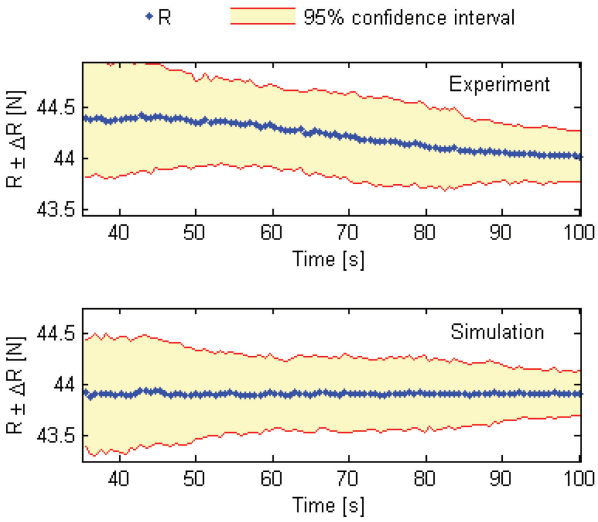

Figure 26 Predicted mean and confidence interval (95%) for resistance data from experiment and simulation using multiple window technique (Steen et al., 2016)

Brouwer & Klinkenberg (2016) investigated the spectral components of the uncertainty spectrum. Using this power spectrum based method, sources of significant uncertainty can be identified and, when avoided, the overall uncertainty can be reduced. While this approach aided reducing uncertainties in the mid-frequency range, low frequency noise was maintained and sources need to be identified.

Low-frequent noise in drag measurements was found to occur due to the unsteadiness of the free surface caused by the acceleration of the model as mathematically predicted by Havelock (1949) and Wehausen (1964). It was related to model testing by Day et al. (2009) and also proven to occur in CFD simulations and for full-scale ships (Haase et al., 2016a). In deep water, this low-frequent noise solely depends on the model speed, while decreasing water depth reduces the frequency and it becomes zero for a depth Froude number of unity.

Some systematical resistance tests have been performed in Ata Nutku Ship Model Testing Laboratory of Istanbul Technical University (ITU) to determine the uncertainties for a displacement type of ship (KCS hull) in (Delen and Bal, 2015). The uncertainty arising from the resistance tests has been estimated and compared according to ITTC 2002 and 2014 regulations (ITTC 2002 and ITTC 2014). It has been found that both ITTC regulations are in good agreement. In the revised regulation (ITTC, 2014), only the dominant components that are important on the results have been taken into consideration. Thus the applicability of the regulation has been improved.

8 TURBULENCE STIMULATION

8.1 Introduction

It is now accepted practice to use turbulence stimulation devices on any model which may experience laminar flow during model tests. An extensive review on historical development and fundamental physics of turbulence stimulators (TS) was conducted by 26th ITTC Resistance Committee (2011) and included in their final report. This included an example approach for evaluating the appropriate model scale resistance correction and suggestions made as to how to more effectively use the procedure that incorporates the application of turbulence stimulation.

A complementary review is conducted by 28th ITTC Resistance Committee, especially focusing on state-of-the-art development since 26th ITTC conference meeting in 2011. Revisions to the relevant procedure 7.5-01-01-01 Ship Models have been proposed, placing more principal description on the application of turbulence stimulators. The occurrence of turbulence stimulation methods in other procedures is also listed.

It is worthwhile restating the reasons that turbulence stimulation is applied to a ship model, which are (in decreasing order of importance): (1) ensure that the flow regime at model scale is equivalent to that at full scale, (2) that the model scale flow is constant and hence repeatable across the range of design Froude numbers and between repeat tests, and (3) that a known scaling approach can be applied.

8.2 Historical Development of Turbulence Stimulation Methods

For a full scale ship, the length based Reynolds number is typically 10^8 or higher, therefore the flow around the entire hull is fully turbulent. For the scaled model during the model test, the length based Reynolds number range is typically from 10^5 to 10^7 (Figure 27), considerable laminar flow can be expected around bow area then by natural transition along the model hull from laminar flow to turbulent flow, if no turbulence stimulator is used (Figure

28). The concern arises when a fully turbulent friction line, such as ITTC 1957 model-ship correlation line is used for scaling the model scale resistance to full scale. The practical answer to the problem is to deliberately "trip" the laminar flow by some kinds of devices near the stem.

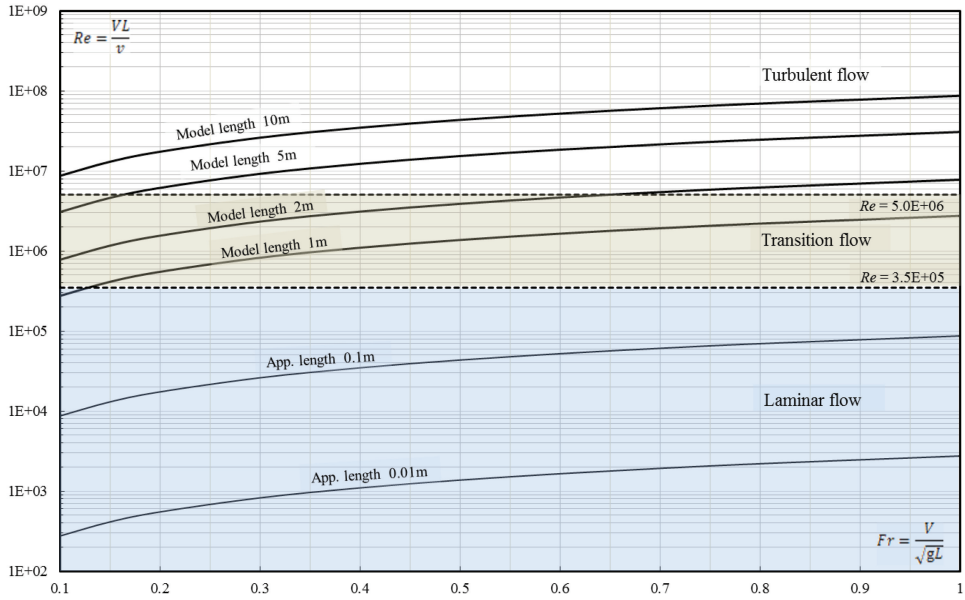

Figure 27 An example for flow regime estimation for typical model/appendage length without turbulence stimulation devices ($\upsilon = 1.1386 \times 10^{-6}$ m^2/s for 15℃ fresh water, $g = 9.8067$ m/s^2)

Trip wires were first used in the Berlin tank as early as 1925 and came into general use there around 1933 (Manen 1988). Since then, various types of turbulence stimulation methods have been adopted (refer Figure 29), including leading rod ahead of the model, trip wire, sand strips, pins or studs, normal plate and slotted strip, etc. (Breslin & Macovsky 1950, Preston 1958), as well as forced vibration of the model, disturbance of the flow by mechanical devices, sound devices, or water jets (Davidson 1951).

The most commonly utilized turbulence stimulators now are studs, wires and sand strips which are described in detail in the ITTC procedure 7.5-01-01-01 Ship Models.

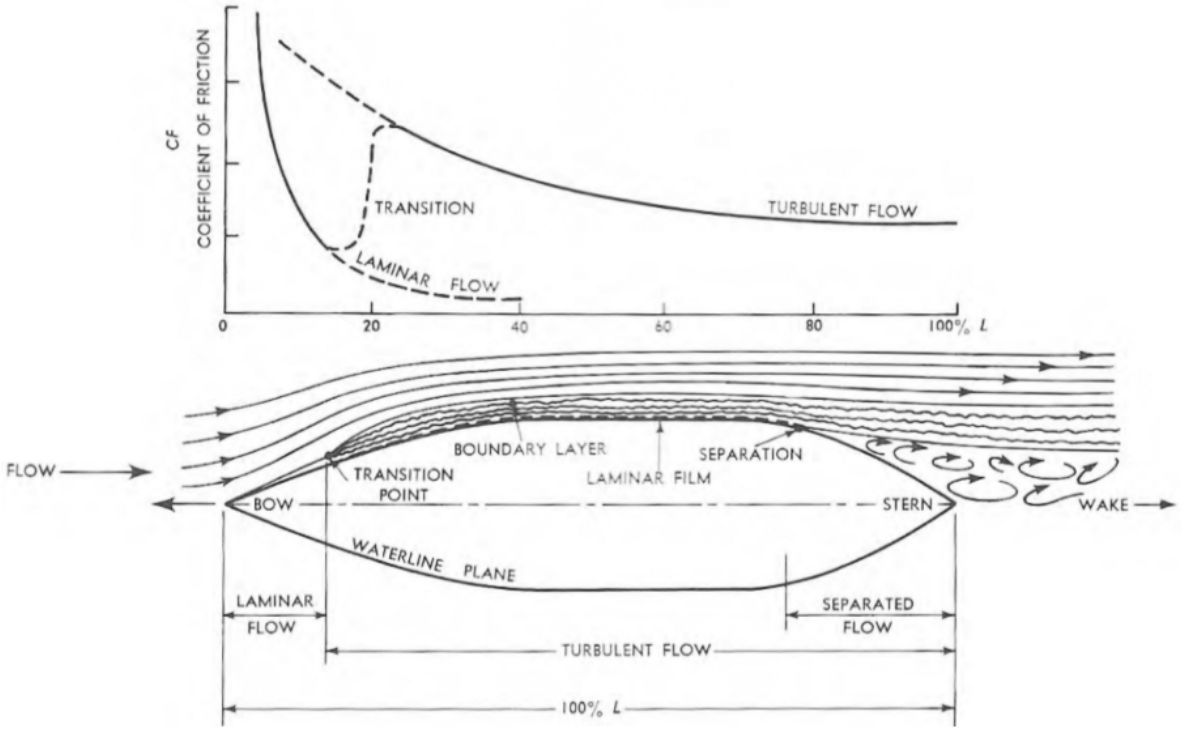

Figure 28 Illustration of the boundary layer development (bottom) around a ship model hull and the related skin friction coefficient for laminar and turbulent flow (Gillmer & Johnson, 1982)

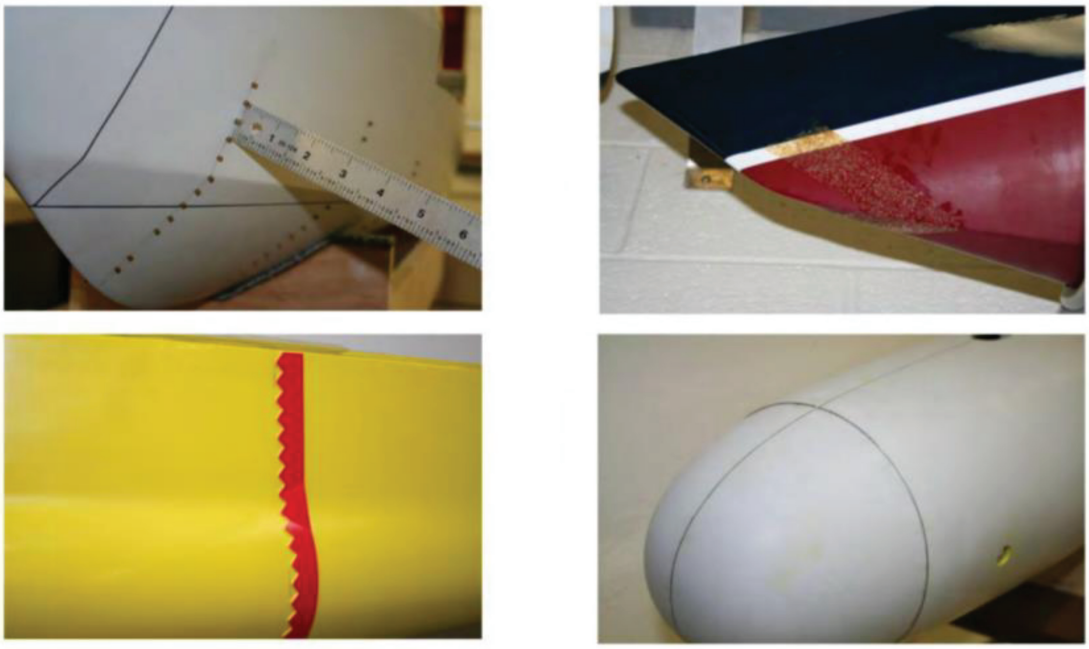

Figure 29 Different turbulent stimulation devices, clockwise from top left: studs, sand strip, trip wire, Hama strips (Murphy 2010)

Turbulence stimulators attached to the model increase the resistance due to its parasitic form drag. The total friction resistance component of the model is equivalent to the sum of the friction resistance of the laminar flow area ahead of the TS, the parasitic drag of TS itself and the friction resistance of the turbulent flow area downstream of the TS. The total friction resistance of the whole model which is covered by the assumed fully turbulent flow, derived from the ITTC 1957 model-ship correlation line formula, should equal to the sum of sectional friction resistance components, if the size and position of the TS is appropriate and no drag correction is made.

An example method of the resistance correction for a unit aspect ratio stud was given in Molland et al. (1994) and also presented in 26th ITTC Resistance Committee final report (Section 6.4). As an example, for model 6b of semi-displacement hull form, the maximum change in model total resistance was 3%.

The studs, typically between 1.6 and 3.2 mm in diameter, 0.5 to 3.0 mm high and spaced between 12 and 25 mm apart, will generate 3D various unsteady vortex structures shown in Figure 30 (Pattenden et al., 2005, Pattenden et al., 2007). Hughes & Allan (1951) derived a minimum distance between the pins (studs, 3.2 mm diameter, 2.5 mm height at 25.4 mm spacing) to the stem that was required for successfully tripping the flow. This work was the basis for tripping guidelines until today (Figure 31).

It is worth checking that the spacing is sufficient otherwise large areas of laminar flow can be created downstream before the turbulent disturbance has spread to the full width.

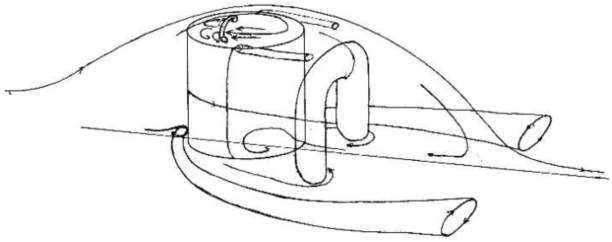

Figure 30 A schematic of typical vertical flow features around an aspect ratio 1 cylinder

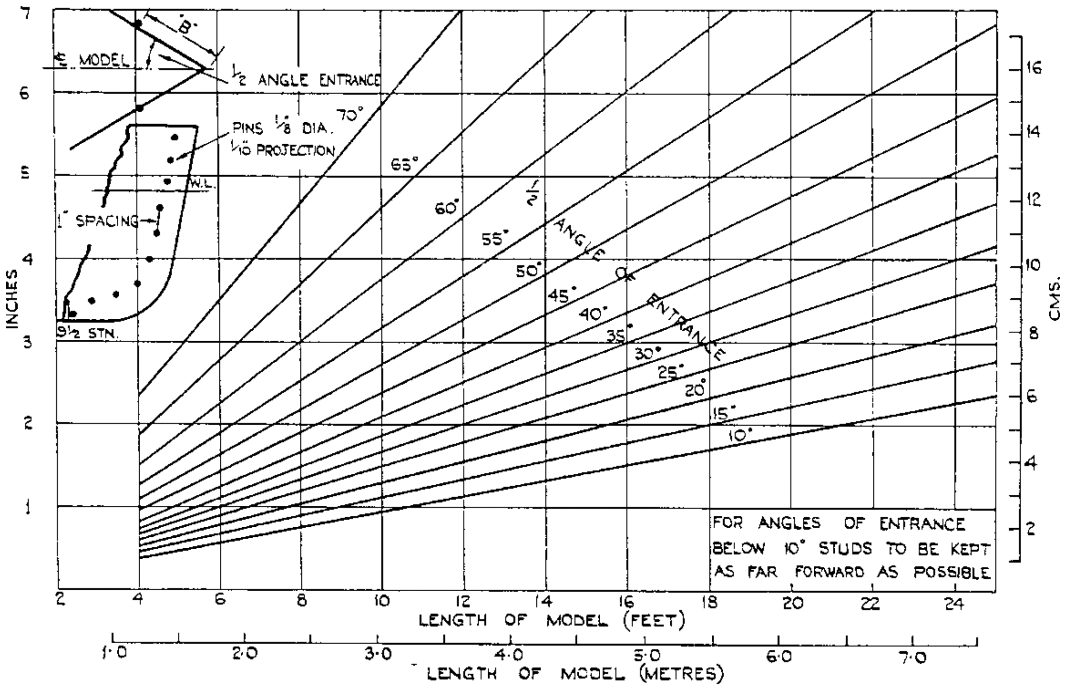

Figure 31 Location of studs as turbulence stimulators (Hughes and Allan, 1951)

The wire, typically between 0.5 mm and 1.0 mm diameter and convenient manufacturing and mounting, will generate turbulence to disturb the laminar flow around bow area without TS. Breslin & Macovsky (1950) investigated the flow regime over the hull of a tanker model with and without wires (0.032 inch) at various speeds using 18 hot-film sensors. Figure 32 shows an example of the extent of laminar flow for a range of speeds with and without trip wires.

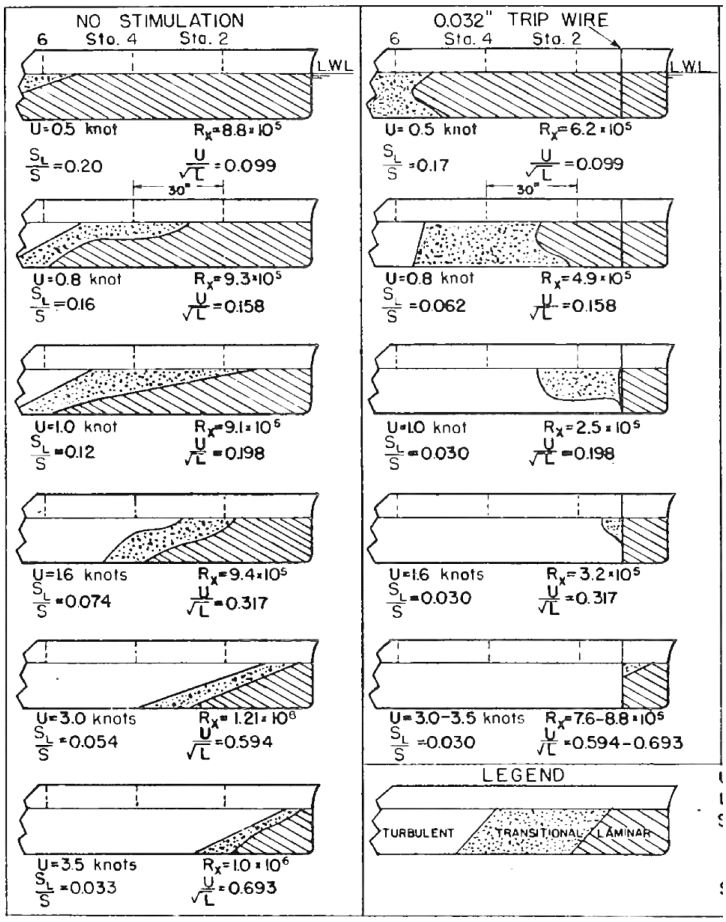

Figure 32 Visualization of laminar, transitional, and turbulent areas on a tanker model without (left) and with (right) trip wires (Breslin & Macovsky, 1950)

Wires are often preferred over other TS devices for convenience, due to their dimensional accuracy and ease of fitting. However, wires are less effective at promoting transition generally.

The sand strip, typically comprise backing strips/adhesive of 5 mm to 10 mm width covered with sharp edged sand with grain size around 0.50 mm. Sand strips are the preferred method of turbulence stimulation for long slender hulls, such as high speed catamarans.

It is better to have a few roughness elements only rather than a high density attached to tape, often the tape thickness itself is sufficient to ensure transition and that use of a serrated tape edge is effective at promoting transition.

For TS around bulbous bows, great care should be taken that the size and number of TS used does not fundamentally alter the bow wave and thus the progressive accumulation of pressure and skin friction resistance along the hull.

Turbulence stimulation should be applied to appendages when laminar flow over the appendage is likely. The approach for the selection of appropriate turbulence stimulation devices for appendages is presented in 26th ITTC Resistance Committee final report (Section 6.5) and provided in the revised Ship Models procedure (7.5-01-01-01).

8.3 Recent Research on Turbulence Stimulation

26th ITTC Resistance Committee final report (2011) presented the fundamental physics reviews on turbulence stimulation methods. The turbulence stimulators acts to mix high momentum flow down into the lower less energetic regions of the boundary layer, and makes the laminar-turbulent transition occurring rapidly and without significantly altering the form drag. The generated disturbances can be associated with various unsteady vortex structures behind a trip stud as shown in Figure 30, those on the 2D flow separation behind a trip wire or the more general generation of disturbances behind multiple elements on a roughness strip.

For flow stimulation around ship models, it is convenient to consider the Reynolds number in different ways:

- Longitudinal Reynolds numbers:

√ length Reynolds number: $Re_L = \frac{VL}{\nu}$

with V being model velocity, L being model length, and ν being the kinematic viscosity

√ local Reynolds number: $Re_x = \frac{Vx}{\nu}$

with x being the longitudinal coordinate aft of the leading edge

- Normal Reynolds numbers:

√ momentum thickness Reynolds number: $Re_\theta = \frac{V\theta}{\nu}$

with θ being the momentum thickness that is defined by: $\theta = \int_0^d \frac{u}{U}\left(1-\frac{u}{U}\right)dy$

and can be approximated by: $\theta = \frac{0.664x}{Re_x^{1/2}}$ (Schlichting and Gersten, 2000)

√ roughness Reynolds number: $Re_k = \frac{u_k k}{\nu}$

with u_k being the model velocity and k the roughness height

√ roughness Reynolds number: $Re_d = \frac{Uk}{\nu}$

with U being the velocity far away from the wall/undisturbed inflow velocity

Murphy (2010) investigated the effect of different thicknesses of Hama strips on the extent of laminar flow on a thickened flat plate and a prismatic ship hull of DARPA shape. Hot-film sensors were used. Without stimulation the flow tripped at Re_θ around 550 on the flat plate and around 350 at the prismatic hull. On both devices, with sufficiently thick strips (7 layers) the flow tripped by $dRe_\theta = 100$ earlier, when compared to not using stimulators.

Jones et al. (2013) tested a submarine model in a wind tunnel at $Re_L = (3.6 - 6.3) \times 10^6$. They compared the effect of a trip wire and sand strips on the skin friction on the body using a Preston-tube. A wire of 0.2 mm diameter and an 80 grit ($k = 0.21$ mm) sand strip were found to correctly trip the flow for $Re_L < 5.4 \times 10^6$, for higher speeds the flow was overstimulated. For a 0.5 mm diameter wire, the flow was overstimulated for 600 wire diameters downstream of the wire. They conclude that

under-stimulation has a more significant effect on the skin friction than over-stimulation, so they suggest to utilize wire diameter Reynolds number of $Re_k = 580-900$ for appropriate stimulation. The sand strip was found to deteriorate during the testing, thus wire stimulators were recommended.

Shen et al. (2015) investigated axis-symmetric bodies and found that a tripping wire of 0.53 mm diameter satisfying $Re_k = 400$ is sufficient to trip the flow when located 5% L aft of the nose.

Hutchison (2014) investigated the scaling effects on a 1/8 scale model of an IACC sailing yacht. Two rows of studs were placed 200 mm apart from each other, with the foremost one being 200 mm aft of the forward perpendicular, corresponding to 6 and 20% L_{PP}. The flow regime was investigated using a Kurtosis analysis of hot-film measurements (Binns et al., 2009). Turbulent flow was concluded for all cases investigated from 2.4×10^4 with turbulence studs used. Without studs the stimulating effect of free surface waves was noted. It was concluded that for this model, when scaling using the Grigson friction line a minimum Reynolds number of 2.6×10^6 ($Fr = 0.27$) should be obeyed.

Lee (2014) used CFD to correlate background turbulence and surface roughness to critical momentum thickness Reynolds numbers, at which the flow over a flat plate trips. According to his results (Figure 33), on a smooth plate the flow trips at Re_θ of 300–400, if the background turbulence is of 2%–2.5%. A rougher surface and more background turbulence reduce the critical momentum thickness Reynolds number. Pearson (2015) used Lee's approach and simulated the flow transition over a fully submerged scale model of a 4.3 m long wave-piercing catamaran. Pearson (2015) found that laminar flow extended to $Re_x = 4 \times 10^5$ (for a flow tripping at $Re_\theta = 320$) on the bow if no stimulation was used, which correlated to hot-film measurements on a scale model (Figure 34). Schnabel (2017) experimentally concluded for laminar areas up to 9×10^5 and also found more turbulent flow close to the free surface, even though no distinct wave-breaking was observed for this hull with very fine angle on entry.

Furthermore, the results of Pearson (2015) suggest that when using a sand patch at the bow for turbulence stimulation, extending from the leading edge to $Re_x = 0.5 \times 10^5$ at 1 m/s, it must have at least an equivalent sand grain roughness of 200 μm for making the flow fully turbulent, however no drag penalty for higher roughness was identified. This can be explained, because the rough patch does not extent into the fully turbulent flow range. Also the simulation results show that the local skin friction coefficient for fully turbulent flow after tripping is higher than that of the fully turbulent flow simulation, which supports the concept of a virtual boundary layer origin being aft of the leading edge (Smits 1982).

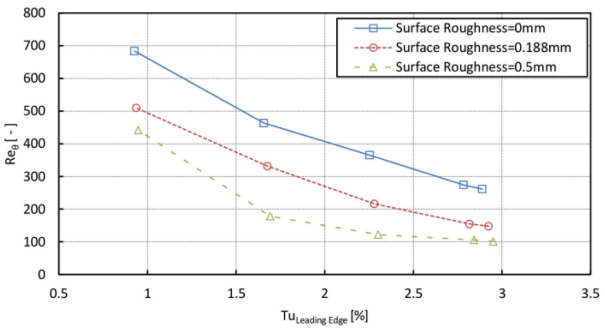

Figure 33 Critical momentum thickness Reynolds number based on CFD simulations for flow over a flat plate for different surface roughness and turbulence intensity (Lee, 2014)

Zurcher (2015) used two rows of studs (at 72 mm and at 434 mm aft of the leading edge) for the above mentioned catamaran demi hull where each row corresponded to Re_θ of 320 for the highest and lowest speed of the investigated range. The 3×3 mm studs were placed 20 mm

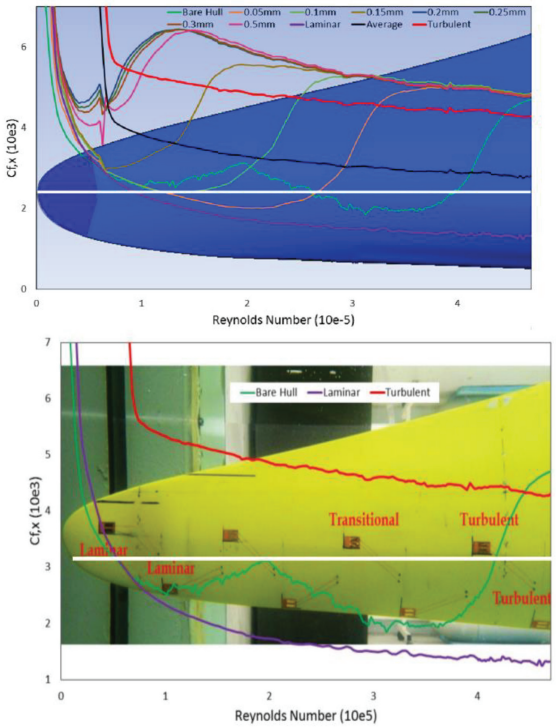

Figure 34 Top: Skin friction coefficient on the bow of a wave-piercing catamaran model (along the white line) for different patch roughness at the leading edge, shown in purple. Bottom: Simulation results and correlation with experimental measurements. The green curve shows the CFD results and the flow type measured at the hot film sensors are written in red text (Pearson 2015)

apart from each other. McDonagh (2016) used different configurations of studs (3×3 mm, 0.6 ×0.6 mm) and sand strips on the same wave-piercing catamaran demi hull. He concluded for sand strips that roughness was secondary to the width of the sand strips for generating turbulent flow. For studs, he found the number is more important than their size to make the flow turbulent. Most effective was a configuration of only one row at 72 mm aft of the bow, with 10 mm stud spacing. From the results of Bradford (2015) and McDonagh (2016), a minimum Reynolds number of $Re_L = 3.2 \times 10^6$ was required to achieve fully turbulent flow for any stimulators used.

8.4 Occurrence Review of TS in ITTC Procedures

All the model test procedures of ITTC framework have been checked for occurrence of TS. And the list of relevant procedures are shown in Table 6. Most procedures refer to the basic procedure provided in Ship Models (7.5-01-01-01), which is revised by adding more principal guidance for the usage of TS by 28th ITTC Resistance Committee. Special TS treatments were found during pod housing unit resistance, and special consideration should be taken during the HSMV resistance and seakeeping tests.

Table 6 List of ITTC procedures which include TS description

Procedure Number	Title	Page No.	Comments
7.5-01-01-01: 2011 Rev.03	Ship Models	4-5	Detailed description on TS, as a reference for other procedures
7.5-02-02-01: 2011 Rev.03	Resistance Test	3, 12	Refer to Ship Models
7.5-02-03-01.1: 2011 Rev.04	Propulsion/Bollard Pull Test	15	Refer to Ship Models
7.5-02-03-01.3: 2008 Rev.00	Propulsion, Performance Podded Propulsion Tests and Extrapolation	9	Artificial roughening on pod housing

7.5-02-05-01: 2008 Rev.02	Testing and Extrapolation Methods High Speed Marine Vehicles Resistance Test	3-4, 12	1) TS applicable for *Re* less than 5×10^6 2) Might be omitted for higher *Re* 3) Trip wires are not recommended 4) TS for appendages out of boundary layer is recommended
7.5-02-05-04: 2014 Rev.01	Testing and Extrapolation Methods High Speed Marine Vehicles Seakeeping Tests	5	If the control system consists of fins, turbulence stimulation should be applied
7.5-02-06-02: 2014 Rev.04	Captive Model Test Procedures	15	Documentation if any
7.5-02-06-01: 2014 Rev.03	Free Running Model Tests	2, 9	Documentation if any
7.5-02-07-04.1: 2008 Rev.02	Testing and Extrapolation Methods Loads and Responses, Stability Model Tests on Intact Stability	3	Turbulence stimulation required for rudders and fins

9 FLOW FIELD VERIFICATION AND VALIDATION PROCEDURE

Assessing the accuracy and uncertainty of detailed flow field data is an impelling necessity for both the numerical and experimental communities due to the expanding use of CFD in ship design and hydrodynamics research and to the increasing demand on reliable experimental data for verification and validation purpose, particularly when complex viscous hydrodynamics is concerned.

Although the argument was tasked to the Specialist Committees on "CFD in Marine Hydrodynamics" and on "Detailed Flow measurement techniques" of the 27th ITTC and some coordinated efforts have been recently conducted under the framework of NATO-AVT on separated flows (Falchi et al., 2016), the verification and validation of the detailed flow field data is still an open issue far from having been addressed that requires further efforts to develop ad-hoc and useful methods able to achieve the right trade-off between technical rigor and practicality.

All that said, the development of a procedure for verification and validation of the detailed flow field data is still premature and needs dedicated, cooperative efforts by experts of both communities to be usefully achieved.

10 BENCHMARK PIV MEASUREMENTS

The "hand-in-hand" relationship between the broadening use of PIV-based techniques within the ITTC organizations and the larger and larger range of practitioners dealing with the application of these techniques has made crucial the need to make benchmark data available for the purpose of verifying the quality of the measurement setups. To this end, due to the inherent differences between a 2C and a SPIV (3C) setup, two different benchmarks have been developed by the ITTC Detailed Flow Measurement Committee in the 26th and 27th ITTC and have been formalized in the procedure 7.5-01-03-04.

The 2C PIV benchmark utilizes a two-component PIV system on a simple 2D geometry consisting of a splitter plate with fence, as shown in Figure 35. The 3C PIV benchmark u-

ses a SPIV system on a more complex 3D flow field generated by a piercing surface flat plate operating at incidence, as shown in Figure 36.

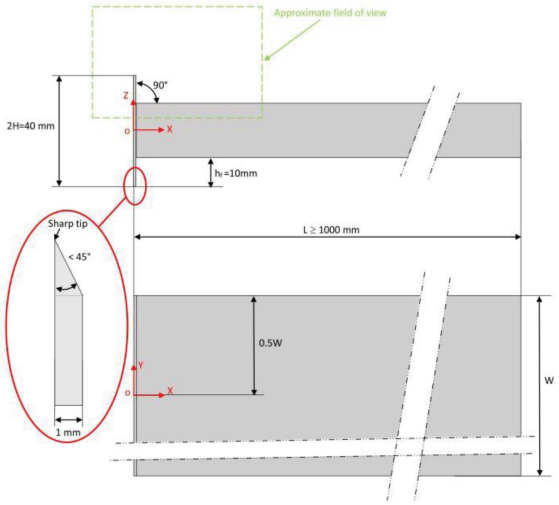

Figure 35 2C PIV benchmark: flow around splitter plate with fence

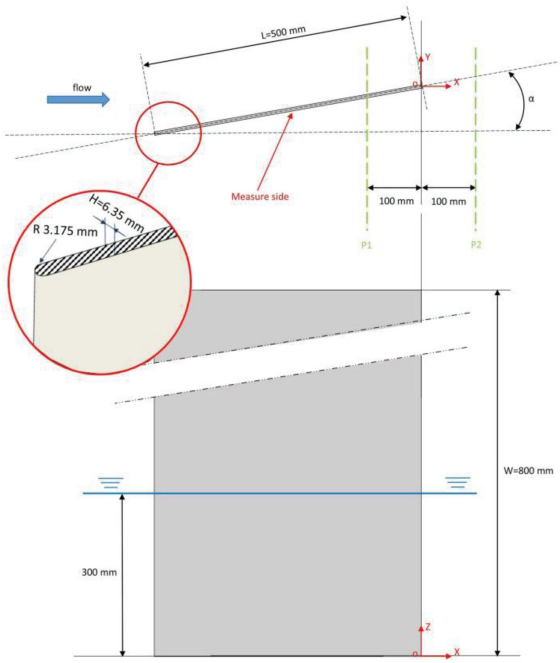

Figure 36 SPIV benchmark: Piercing surface flat plate at incidence

The two benchmarks have been basically intended:

- to ensure that the measurement set up (e.g. cameras, light sheet, seed characteristics, etc.) meet specifications;
- to provide new users of the PIV technique with an indication of how successfully the measurement technique has been implemented in all its steps. This implies that all relevant aspects of the test must be made available to any member organization partaking in the benchmark tests by a dedicated repository. Of specific interest are, for example, the PIV images and the processed results, such that participants can not only compare their own images, but also their PIV processing algorithms on other image sets;
- to give new users the opportunity to evaluate and compare their measurement setup with other established institutions.

The establishment of the PIV and SPIV benchmarking tests has been initiated by the 28th ITTC Resistance Committee through a revision of the procedure 7.5-01-03-04. This has involved clear instructions for performing the benchmark test including details about the model to be used, the measurement conditions and the measurement parameters, as shown in Table 7 and Table 8. Further, the revised 7.5-01-03-04 procedure provides details about the organization of the benchmark program along with information about the conditions to access to the repository and to store the data.

Benchmark data is accessible at this URL: http://www.ittc-benchmark.cnr.it. Access is open to any ITTC participant organization that uploads or has already uploaded its database and is conditioned upon the compilation of a questionnaire with personal information (i.e. name, affiliation, etc.) and details about the database to be uploaded (e.g. benchmark type, experimental rig, image calibration and processing procedure, etc.). The primary purpose of the questionnaire, is to provide any user with all the relevant information about the experimental campaign.

Table 7 2C PIV benchmark specifications

Table 7-2C PIV benchmark specifications

Geometry and material	2H	40mm
	h_f	10 mm
	L	>100 h_f
	W	Large enough to avoid 3d effect in the measurement section
	Material	Aluminium or steel
Field of view and plane position	Out of plane position of measurement plane	Z=0
	Recommended field of view (minimum size)	-1.5 h_f<X<4.5 h_f 0.5 h_f<Y<4.5 h_f
Measurement Conditions	U_∞	5m/s (low speed) or 10 m/s (high speed)
PIV image Format	TIFF or BMP	
Vector field **Format**	X (mm), Y (mm), Z (mm), U (m/s), V (m/s)	

Table 8 3C PIV benchmark specifications

Geometry and material	L		500 mm
	W		800 mm
	H		6.35 mm
	Material		steel
Field of view and plane position	Plane P1	Out of plane position	x=-100 mm
		Recommended field of view (approximatively)	-150 mm<Y<150 mm -100 mm<Z<100 mm
	Plane P2	Out of plane position	x=100 mm
		Recommended field of view (approximatively)	-150 mm<Y<150 mm -100 mm<Z<100 mm
Measurement conditions	U_∞		0.4m/s (towing tank) or 2 m/s(free surface channel)
	A		20 deg (towing tank) or 5 deg (free surface channel)
PIV image format	TIFF or BMP		
Vector field format	X (mm), Y (mm), Z (mm), U (m/s), V (m/s), W(m/s)		

The revised 7.5-01-03-04 procedure is organized into 5 main sections and 3 appendices and covers all aspects of performing a benchmark test, including setup and presentation of the results, data uploading and downloading.

Sections 1 and 2 of the procedure report the purpose and scope of the benchmark tests.

Section 3 presents the main requirements and objectives of the PIV and SPIV benchmark tests.

Section 4 presents the PIV and SPIV benchmark studies including a detailed description of the two setups. Results from institutions that have performed the benchmark tests are also presented in this section as examples.

Section 5 describes the organizational structure of the repository. A schematic representation of the repository organization and access procedure is shown in Figure 37 and Figure 38.

The three appendices report the questionnaire (Appendix A) and all the instructions on performing the tests (Appendix B) and delivering the data (Appendix C).

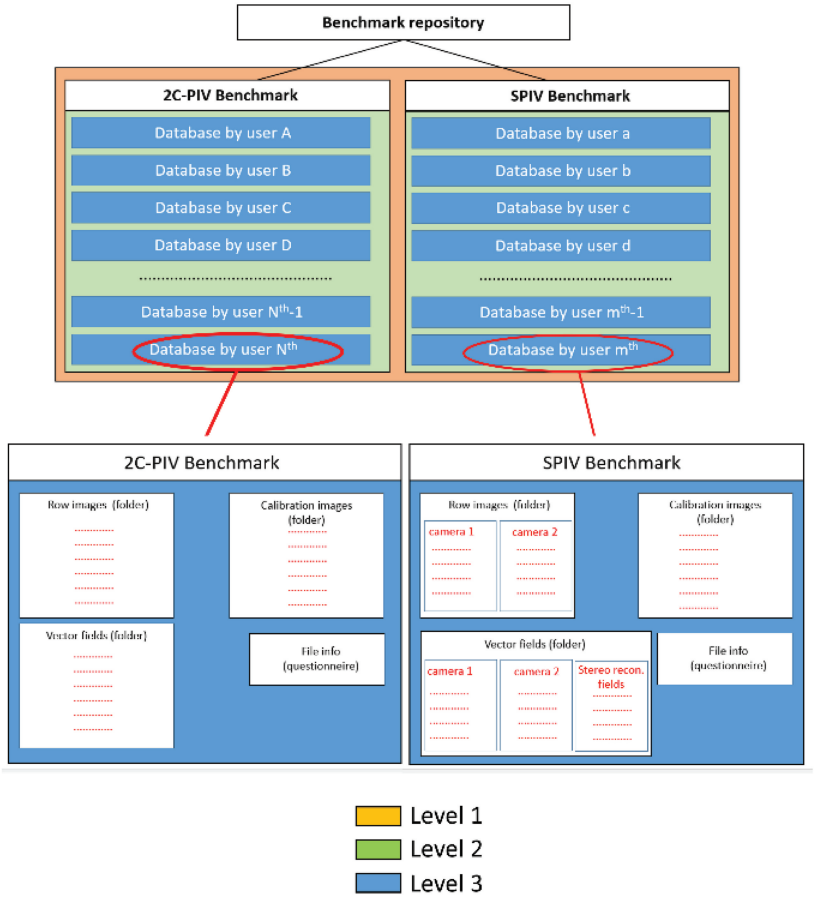

Figure 37 Repository organization

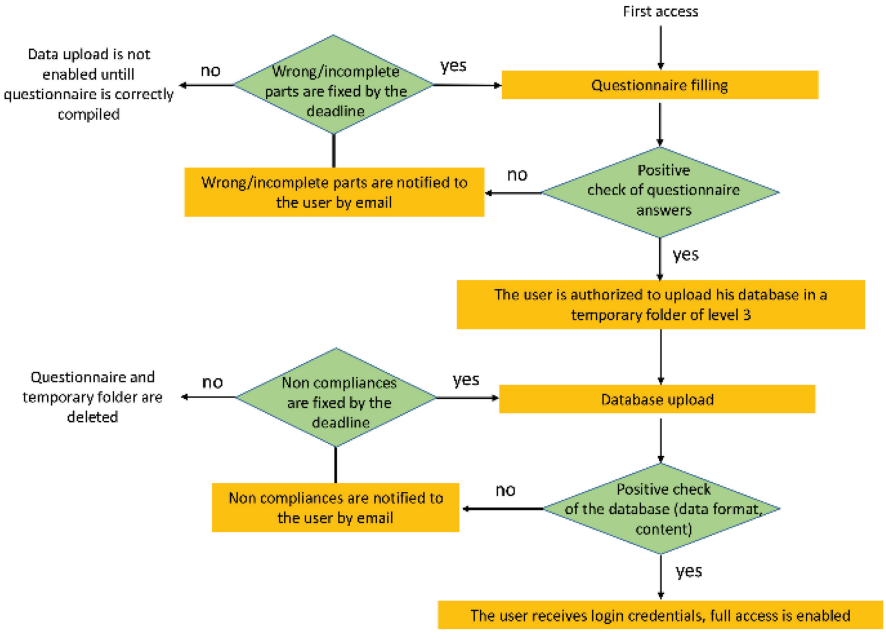

Figure 38 Repository access procedure

11 TEST DATA

11.1 World Wide Campaign

The 24th ITTC Resistance Committee initiated a worldwide series of comparative resistance tests for identifying facility biases under the framework of ITTC procedures for uncertainty analysis. They invited all ITTC members to participate in the task by performing resistance tests on one of two geosims of the DTMB 5415 Combatant having lengths of 5.720 and 3.048 metres respectively. A technical procedure was created, including data submission guidance to preserve the confidentiality of the data.

Progress and analyses from the worldwide campaign has been reported each Resistance Committees from the 24th to 27th ITTC. The final report of the 27th ITTC Resistance Committee presented a summary of the inter-laboratory comparison of the data provided by 11 towing tanks for the large model. The present report presents a similar summary for the small model.

Inter-laboratory campaign (small model, LBP = 3.048 m). The comparison of all available test data from a total of 10 towing tanks for the small model of DTMB 5415 has been performed. The small model, denoted as Geosim B, is a wooden geosim of the model DTMB 5415, with the following particulars in calm water without trim (corresponding to a scale of 46.588): L_{pp} of 3.048 m, draft of 0.132 m, wetted surface area of 1.3707 m^2, displacement volume of 0.0826 m^3(ITTC, 2005). Further details of the hull form are available on the NMRI web site (NMRI).

As prescribed by the ITTC comparative tests, there would be 9 repeat tests at each speed in each towing tank to perform statistical analysis (note: not all tanks performed all 3 speeds). All the total resistance measurements in a specific tank are corrected to each of the three the nominal speeds (Fr = 0.1, 0.28 and 0.41) and converted to the nominal temperature for fresh water of 15 degrees Celsius before any statistical analysis is made.

The means of total resistance coefficients from those repeat tests in each tank are given in Table 9 as similar to large model as given in the 27th ITTC. Such means can be regarded as the best measurement in each towing tank. After computing the average of each experiment set, the general average and standard deviation of the corresponding towing tank are found. The experimental standard deviation (StDev) of tests in each tank is also presented. Such standard deviations can be used to estimate the uncertainties of repeatability of measurement in each towing tank.

The practical approach to detect outliers is applied for intra-laboratory comparisons as in the 27th ITTC and they are given as the following steps for the completeness of the report:

Step 1: Calculate the mean (R_0) and standard deviation (S_0) of 9 repeat tests,

$$R_0 = \frac{1}{N}\sum_{k=1}^{N} R_i \quad (i = 1, 2, \cdots, N) \tag{3}$$

$$S_0 = \left\{ \frac{1}{N\text{-}1}\sum_{i=1}^{N} (R_i\text{-}R_0)^2 \right\}^{1/2} \quad (i = 1, 2, \cdots, N) \tag{4}$$

Step 2: Decide if there is any test result outside the scattering band of double deviation,

$$|R_i\text{-}R_0| \leqslant 2\, S_0 \quad (i = 1, 2, \cdots, N) \tag{5}$$

Step 3: If no test is outside the band, no outlier exists. If the kth test is outside the "double" band, it will be doubted as an outlier. Tick it out and calculate the mean (R_*) and standard deviation (S_*) of the repeat tests again, excluding the kth test.

Table 9 Statistical analysis of resistance measurement in comparative tests of the small DTMB 5415 model in 10 towing tanks

Tank No	$C_T \times 10^3$_15deg_Fresh Water of Small Model (3.048)_ DTMB 5415_S=1.371 m^2					
	Fr = 0.1		***Fr*** = 0.28		***Fr*** = 0.41	
	Mean	**StDev**	**Mean**	**StDev**	**Mean**	**StDev**
# 1			**4.877**	**0.60%**	**6.659**	**2.12%**
# 2	5.300	3.81%	5.463	0.84%	7.985	0.50%
# 3	5.441	2.57%	5.466	0.43%	8.255	0.47%
# 4	4.414	8.29%	5.240	1.02%	**7.024**	**2.97%**
# 5	5.362	4.03%	5.412	0.71%	7.891	0.38%
# 6	5.367	2.59%	5.412	0.71%	7.891	0.38%
# 7					7.706	1.53%
# 8	5.477	4.50%	5.357	0.98%	7.730	0.85%
# 9	5.266	1.77%	5.303	0.80%	7.533	0.72%
# 10	4.412	4.72%	5.282	2.39%	7.831	2.62%
Baseline	5.130	8.73%	5.367	1.59%	7.853	2.73%
Averaged after outliers (in RED) ticked out						

Step 4: Judge if the k^{th} test is outside the scattering band of triple deviation,

$$|R_k - R_*| \leqslant 3 S_* \tag{6}$$

Step 5: If the k^{th} test is outside the "triple" band, its measurement can be considered as an outlier and then the mean R_* and standard deviation S_* are adopted as statistic parameters of repeat tests. Otherwise, no outlier is detected and the mean R_0 and standard deviation S_0 of repeat tests are used. For inter-laboratory comparison, the average of measurement means of 10 towing tanks can be considered as a kind of baseline.

When averaging the means of tests in 10 tanks, the detection of outlier can be performed following the above steps. The statistical analysis and corresponding results are shown in Figure 39-43 and Table 9. These deviations are kind of measure for the facility bias. It is interesting to note that the scattering of data between towing tanks is much smaller as Froude number is increasing.

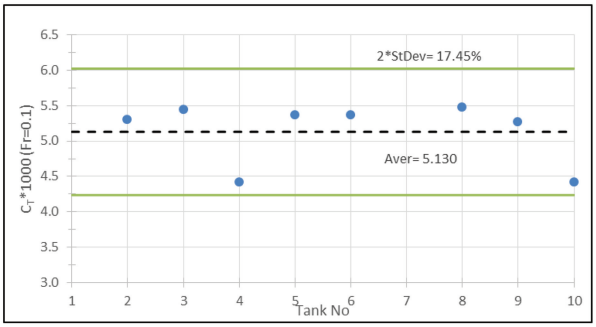

Figure 39 Statistical analysis for means of total resistance coefficients of 8 tanks (Fr = 0.1, no outlier)

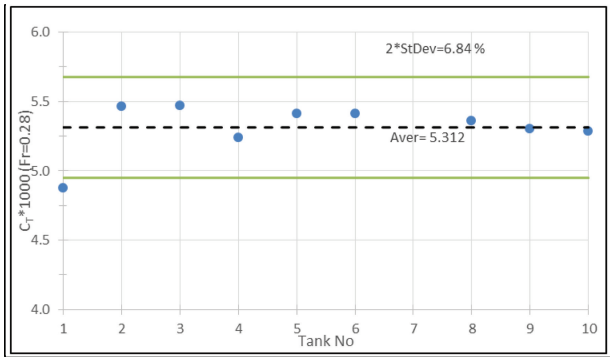

Figure 40 Statistical analysis for means of total resistance coefficients of 9 tanks (Fr = 0.28, no outlier)

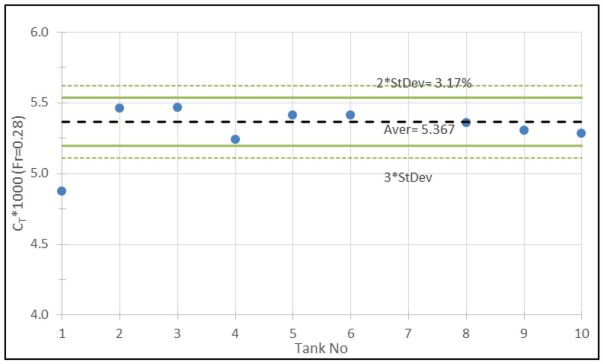

Figure 41 Statistical analysis for means of total resistance coefficients of 9 tanks (Fr = 0.28,excluding one outlier)

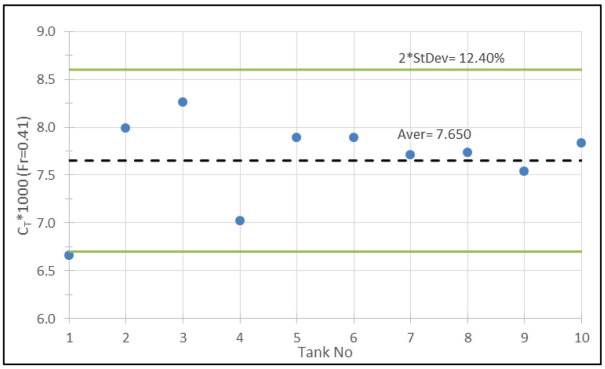

Figure 42 Statistical analysis for means of total resistance coefficients of 10 tanks (Fr = 0.41, no outlier)

Figure 44 where it is shown that the scattering band of overall average is larger than that of small model as given in the 27th ITTC, when the outlier is excluded.

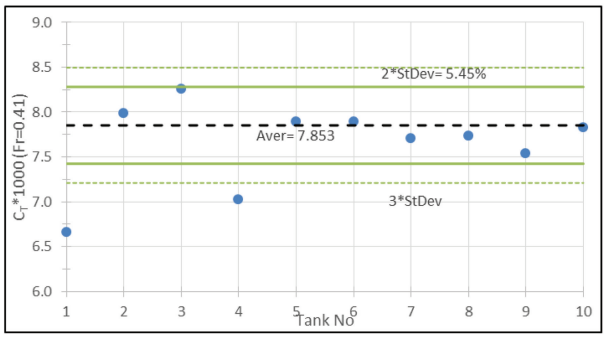

Figure 43 Statistical analysis for means of total resistance coefficients of 10 tanks (Fr = 0.41, excluding outliers)

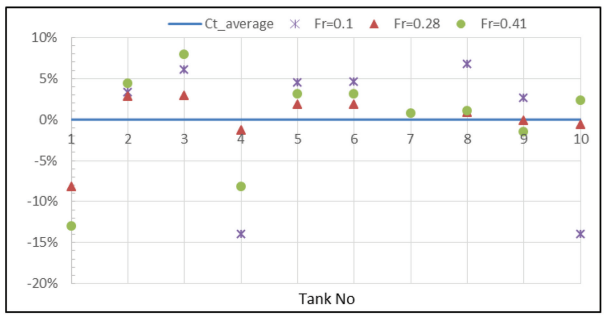

Figure 44 Scattering of means of resistance by 10 towing tanks in comparative tests of the small DTMB 5415 model

The measurements of running sinkage and trim would present more information to intra and inter-laboratory comparison of resistance tests. For intra-laboratory comparison, the statistical analysis given in (Olivire et al, 2001) for sinkage and trim from repeat tests in each towing tank is given in Tables 2 to 5. Obviously, the scattering of resistance is not closely correlated to that of sinkage.

For intra-laboratory comparison the statistical analysis for means of sinkage and trim from repeat tests in each towing tank is shown in Figures 45-50 and also presented in Tables 10-12. The scattering of resistance is not closely correlated to that of trim, either, as shown in Figure 51. Note that the standard deviation for the lowest speed (Fr = 0.1) is higher due to the very limited number of tank results. The sinkage value given by 10th tank has been treated as an outlier.

Table 10 Statistical analysis of running sinkage and trim measurement in comparative tests of the small DTMB 5415 model (Fr=0.1)

Ct×10³_15deg_Fresh Water of Small Model DTMB 5415 L_{pp}=3.048 m; S=1.371 m²					
Resistance (Ct×10³)		**Sinkage (mm)**		**Trim (deg)**	
Mean	**StDev**	**Mean**	**StDev**	**Mean**	**StDev**
N/A		N/A		N/A	
5.300	3.81%	N/A		N/A	
5.441	2.57%	−0.127	0.173	−0.026	0.004
4.414	8.29%	N/A		N/A	
5.362	4.03%	N/A		N/A	
5.367	2.59%	N/A		N/A	
N/A		N/A		N/A	
5.477	4.50%	−0.106	0.173	−0.020	0.006
5.266	1.77%	N/A		N/A	
4.412	4.72%	**−0.994**	**0.340**	−0.015	0.002
5.130	8.73%	−0.116	0.015	−0.020	0.006
Averaged after outliers (in RED) ticked out					

Table 11 Statistical analysis of running sinkage and trim measurement in comparative tests of the small DTMB 5415 model (Fr=0.28)

Fr=0.28 Tank No	Ct×10³_15deg_Fresh Water of Small Model DTMB 5415 L_{pp}=3.048 m; S=1.371 m²					
	Resistance (Ct×10³)		**Sinkage (mm)**		**Trim (deg)**	
	Mean	**StDev**	**Mean**	**StDev**	**Mean**	**StDev**
# 1	**4.877**	**0.60%**	N/A		N/A	
# 2	5.463	0.84%	−6.090	0.852	−0.086	0.031
# 3	5.466	0.43%	−5.626	0.313	−0.120	0.019
# 4	5.240	1.02%	N/A		N/A	
# 5	5.412	0.71%	N/A		N/A	
# 6	5.412	0.71%	N/A		N/A	
# 7	N/A		−7.902	0.110	−0.144	0.016
# 8	5.357	0.98%	−4.762	0.197	−0.099	0.007
# 9	5.303	0.80%	−4.890	0.392	−0.098	0.007
# 10	5.282	2.39%	−6.440	0.298	−0.123	0.008
Baseline	5.367	1.59%	−5.952	1.158	−0.112	0.021
Averaged after outliers (in RED) ticked out						

Table 12 Statistical analysis of running sinkage and trim measurement in comparative tests of the small DTMB 5415 model (Fr=0.41)

Fr=0.41 Tank No	Ct×10³_15deg_Fresh Water of Small Model DTMB 5415 L_{pp}=3.048 m; S=1.371 m²					
	Resistance (Ct×10³)		**Sinkage (mm)**		**Trim (deg)**	
	Mean	**StDev**	**Mean**	**StDev**	**Mean**	**StDev**
# 1	**6.659**	**2.12%**	N/A		N/A	
# 2	7.985	0.50%	−14.964	0.966	0.457	0.036
# 3	8.255	0.47%	−16.467	1.025	0.498	0.055
# 4	**7.024**	**2.97%**	N/A		N/A	
# 5	7.891	0.38%	N/A		N/A	
# 6	7.891	0.38%	N/A		N/A	
# 7	7.706	1.53%	−17.216	0.226	0.387	0.012
# 8	7.730	0.85%	−14.270	0.164	0.315	0.010
# 9	7.533	0.72%	−12.558	0.575	0.387	0.013
# 10	7.831	2.62%	−15.812	0.535	0.423	0.017
Baseline	7.853	2.73%	−15.214	1.511	0.41	0.06
Averaged after outliers (in RED) ticked out						

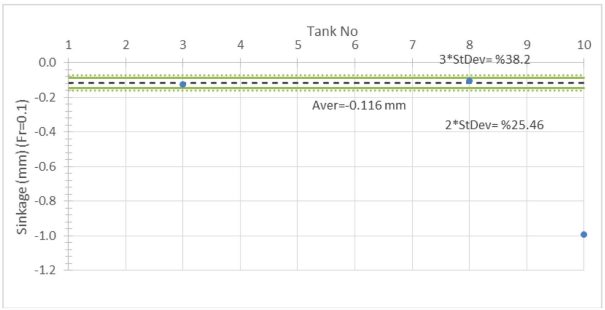

Figure 45 Statistical analysis of running sinkage measurement in comparative tests of the small DTMB 5415 model (Fr=0.1)

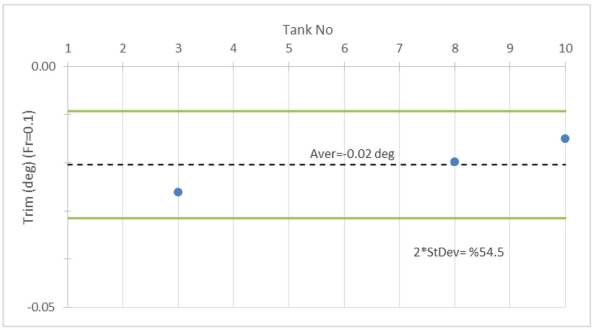

Figure 46 Statistical analysis of running trim measurement in comparative tests of the small DTMB 5415 model (Fr=0.1)

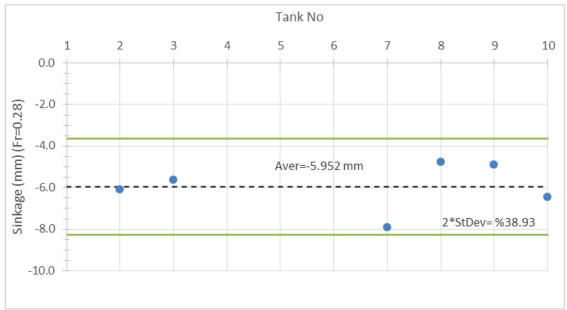

Figure 47 Statistical analysis of running sinkage measurement in comparative tests of the small DTMB 5415 model (Fr = 0.28)

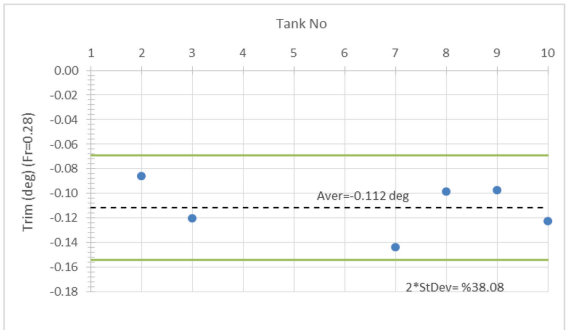

Figure 48 Statistical analysis of running trim measurement in comparative tests of the small DTMB 5415 model (Fr=0.28)

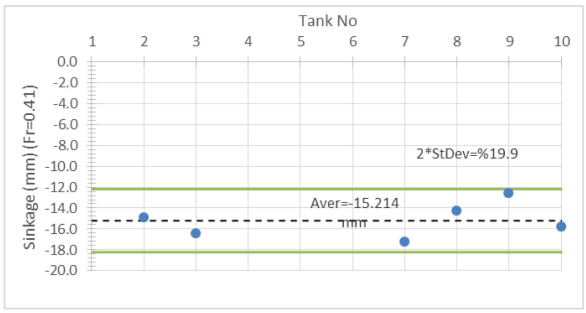

Figure 49 Statistical analysis of running sinkage measurement in comparative tests of the small DTMB 5415 model (Fr=0.41)

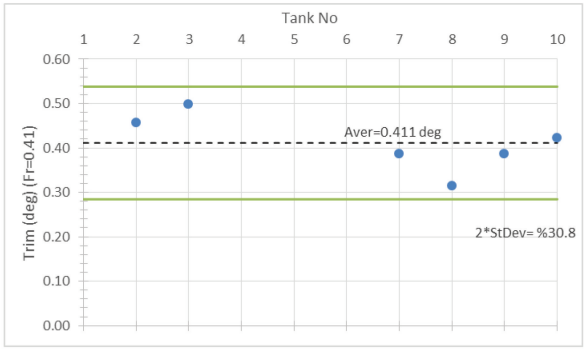

Figure 50 Statistical analysis of running trim measurement in comparative tests of the small DTMB 5415 model (Fr=0.41)

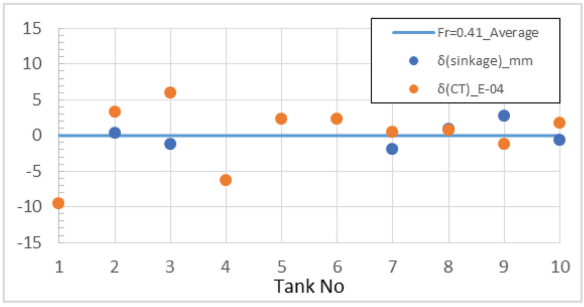

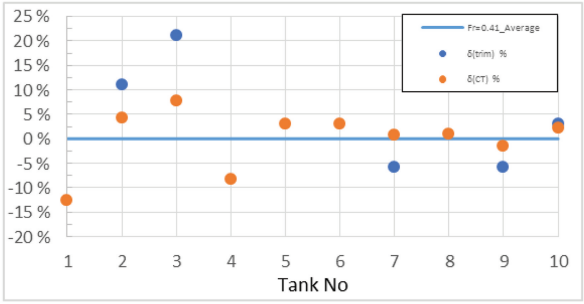

Figure 51 Correlation analysis of resistance to sinkage and trim measurement in comparative tests of the small DTMB 5415 model (Fr=0.41)

The mean values and standard deviations of the tank results (resistance, sinkage, trim) of the small model for Froude numbers 0.1, 0.28 and 0.41 are given as compared with those of large model in Table 13, Table 14 and Table 15, respectively.

Table 13 Comparison of tank results for large and small models at $Fr=0.1$

Large Model (5.72 m)_DTMB 5415							Small Model (3.048 m)_DTMB 5415						
$Fr=0.1$ Tank No	Resistance ($C_T\times10^3$)		Sinkage (mm)		Trim (deg)		$Fr=0.1$ Tank No	Resistance ($C_T\times10^3$)		Sinkage (mm)		Trim (deg)	
	Mean	StDev	Mean	StDev	Mean	StDev		Mean	StDev	Mean	StDev	Mean	StDev
# 1	3.956	1.20%	**-1.64**	0.31	-0.015	0.002	# 1	N/A					
# 2	3.917	1.60%	-1.05	0.40	-0.008	0.006	# 2	5.300	3.81%	N/A			
# 3	4.004	0.90%	-1.19	0.08	-0.012	0.001	# 3	5.441	2.57%	-0.127	0.173	-0.026	0.004
# 4	**4.306**	3.60%	-0.85	0.24	-0.018	0.011	# 4	4.414	8.29%	N/A			
# 5	4.008	1.20%	N/A				# 5	5.362	4.03%	N/A			
# 6	3.918	1.10%	N/A				# 6	5.367	2.59%	N/A			
# 7	N/A						# 7	N/A					
# 8	3.959	0.50%	-1.30	0.03	-0.012	0.000	# 8	5.477	4.50%	-0.106	0.173	-0.020	0.006
# 9	4.001	1.90%	N/A				# 9	5.266	1.77%				
# 10	(#4)						# 10	4.412	4.72%	**-0.994**	**0.340**	-0.015	0.002
# 11	3.989	1.10%	-0.89	0.31	-0.014	0.001	Baseline	5.130	8.73%	-0.116	0.015	-0.020	0.006
# 12	4.019	2.30%	N/A										
Baseline	3.975	0.97%	-1.06	0.19	-0.013	0.004							
Averaged after outliers (in RED) ticked out													

Table 14 Comparison of tank results for large and small models at $Fr=0.28$

Large Model (5.72 m)_DTMB 5415							Small Model (3.048 m)_DTMB 5415						
$Fr=0.28$ Tank No	Resistance ($C_T\times10^3$)		Sinkage (mm)		Trim (deg)		$Fr=0.28$ Tank No	Resistance ($C_T\times10^3$)		Sinkage (mm)		Trim (deg)	
	Mean	StDev	Mean	StDev	Mean	StDev		Mean	StDev	Mean	StDev	Mean	StDev
# 1	4.156	0.20%	-10.95	0.29	-0.113	0.002	# 1	**4.877**	**0.60%**	N/A			
# 2	4.160	0.50%	-10.75	0.43	-0.103	0.005	# 2	5.463	0.84%	-6.090	0.852	-0.086	0.031
# 3	4.216	0.20%	-10.49	0.11	-0.102	0.002	# 3	5.466	0.43%	-5.626	0.313	-0.120	0.019
# 4	4.270	1.80%	-10.39	0.30	-0.111	0.009	# 4	5.240	1.02%	N/A			
# 5	4.248	0.40%	-9.21	0.14	-0.098	0.003	# 5	5.412	0.71%	N/A			
# 6	4.234	0.60%	-12.59	0.19	-0.118	0.003	# 6	5.412	0.71%	N/A			
# 7	4.263	0.40%	-10.23	0.16	-0.104	0.002	# 7	N/A		-7.902	0.110	-0.144	0.016
# 8	4.166	0.50%	-10.34	0.10	-0.101	0.001	# 8	5.357	0.98%	-4.762	0.197	-0.099	0.007
# 9	4.216	0.70%	-10.32	0.35	-0.097	0.004	# 9	5.303	0.80%	-4.890	0.392	-0.098	0.007
# 10	(#4)						# 10	5.282	2.39%	-6.440	0.298	-0.123	0.008
# 11	4.190	0.40%	-10.05	0.30	-0.015	0.004	Baseline	5.367	1.59%	-5.952	1.158	-0.112	0.021
# 12	4.203	0.70%	-9.35	0.15	-0.016	0.002							
Baseline	4.211	0.96%	-10.21	0.552	-0.089	0.037							
Averaged after outliers (in RED) ticked out													

Table 15 Comparison of tank results for large and small models at $Fr=0.41$

Large Model (5.72 m)_DTMB 5415							Small Model (3.048 m)_DTMB 5415						
$Fr=0.41$ Tank No	Resistance ($C_T\times10^3$)		Sinkage (mm)		Trim (deg)		$Fr=0.41$ Tank No	Resistance ($C_T\times10^3$)		Sinkage (mm)		Trim (deg)	
	Mean	StDev	Mean	StDev	Mean	StDev		Mean	StDev	Mean	StDev	Mean	StDev
# 1	6.429	0.20%	−27.35	0.25	0.335	0.012	# 1	**6.659**	**2.12%**	N/A			
# 2	6.497	0.50%	−26.30	0.33	0.373	0.004	# 2	7.985	0.50%	−14.964	0.966	0.457	0.036
# 3	6.536	0.20%	−26.67	0.16	0.430	0.004	# 3	8.255	0.47%	−16.467	1.025	0.498	0.055
# 4	6.587	1.90%	−25.96	0.51	0.415	0.019	# 4	**7.024**	**2.97%**	N/A			
# 5	6.617	0.30%	−22.52	0.12	0.361	0.005	# 5	7.891	0.38%	N/A			
# 6	6.639	0.30%	−29.45	0.28	0.535	0.009	# 6	7.891	0.38%	N/A			
# 7	6.480	0.50%	−24.40	0.16	0.403	0.009	# 7	7.706	1.53%	−17.216	0.226	0.387	0.012
# 8	6.336	0.80%	−25.21	0.07	0.367	0.005	# 8	7.730	0.85%	−14.270	0.164	0.315	0.010
# 9	6.590	1.90%	N/A				# 9	7.533	0.72%	−12.558	0.575	0.387	0,013
# 10	(#4)						# 10	7.831	2.62%	−15.812	0.535	0.423	0.017
# 11	6.412	0.20%	−25.24	0.08	0.378	0.006	Baseline	7.853	2.73%	−15.214	1.511	0.41	0.06
# 12	6.368	0.70%	−24.39	0.20	0.352	0.004							
Baseline	6.499	1.60%	−25.749	1.889	0.399	0.062							
Averaged after outliers (in RED) ticked out													

It is noted that the standard deviations of the total resistance coefficients of the large model are lower than those of the small model. Since the relative effect of the uncertainties will be different for both models, the results of the small model were found to be more scattered. The present uncertainties of towing tanks and the effects of them on the results should be further investigated.

The limited number of sinkage and trim data at the slowest speed ($Fr=0.1$) would be increased to improve the reliability of the results. The standard deviation of total resistance coefficient for increasing Fr numbers is decreasing as opposed to that in large model. On the other hand, since the uncertainties are dominant at low Fr, the standard deviation for small model is higher than that of large model. The present uncertainties of towing tanks and the effects of them on the results should be further investigated. The scattering of resistance is not closely correlated to that of sinkage and trim, either, as shown in Figure 51.

12 RECOMMENDATIONS

The 28th ITTC Resistance Committee recommends the following:

(1) Recommend that ITTC adopt the following updated procedures:

- 7.5-01-01-01 Ship Models
- 7.5-01-03-04 Benchmark for PIV(2C) and SPIV(3C) setups
- 7.5-02-02-01 Resistance Test
- 7.5-02-05-01 High Speed Marine Vehicle Resistance Test
- 7.5-03-01-01 Uncertainty Analysis in CFD Verification and Validation Methodology and Procedures
- 7.5-03-01-02 Uncertainty Analysis in

CFD, Guidelines for RANS Codes

- 7.5-03-02-01 Uncertainty Analysis in CFD Examples for Resistance and Flow

- 7.5-03-02-02 Benchmark Database for CFD Validation for Resistance and Propulsion

(2) Recommend an ITTC committee be formed on methodological processes.

(3) The worldwide campaign data should be disclosed via ITTC official website. We suggest providing a searchable spreadsheet for use of data. No new data was received. The number of tests particularly for sinkage and trim would be increased to improve the reliability of the results. The uncertainties of towing tanks and the effects of them on the results (especially on sinkage and trim values) should also be further investigated.

13 CONCLUSIONS

13.1 Task 1

The Committee identified new experimental approaches which have been proposed to collect and monitor biofilm growth and assess their effect on the frictional drag characteristics. The use of convectional approaches based on resistance measurements has been improved through dedicated apparatuses minimizing any interference and other uncertainty sources, included the human factor. Some advances have been made in the assessment of the roughness and coating application characteristics.

The Committee added new benchmark data to the procedure 7.5-03-02-02: CFD, Resistance and Flow Benchmark Database for CFD Validations for Resistance and Propulsion.

CFD can be a reliable tool to determine the drag of marine surface craft, as the relevant flow phenomena are resolved. However, in comparison to model scale experiments 3−8% of deviation in drag may still occur.

13.2 Task 2

All ITTC Recommended Procedures relevant to resistance and resistance specific CFD procedures that were not reviewed during the 27th ITTC have been reviewed and updated in the light of current practice. Also included was Recommended Procedure 7. 5-01-01-01 Ship Models, which was updated to incorporate aspects of the RC tasks related to hull surface roughness, turbulence stimulation and the use of rapid prototyping for manufacturing models and appendages.

13.3 Task 3

The committee investigated the influence of the surface roughness of the model ship used in the towing tank test on the resistance measurement result. Regarding the samples of various materials used for model ships, the roughness of the ISO method was measured using a direct contact type roughness measuring device. Assuming the obtained roughness height to be equal to the sand roughness height, the increment of the frictional resistance due to the roughness can be estimated based on the turbulent boundary layer theory with respect to the flat plate, using White's equation about the sand roughness. By using this method, in addition to paraffin, or wood, or metal, or foamed urethane, which have been used as a material for model ships in the past, new materials used for so-called 3D, which are gradually being used recently. So, each organization can evaluate the magnitude of roughness influence, or determine the roughness criteria to minimize the influence on the towing tank test.

13.4 Task 6

The roughness of models and appendages produced by rapid prototyping was reviewed, including a survey of test samples produced by multiple 3D printers, including manufacturing process variables such as: material, print speed and print orientation. It was found that the raw surface finish of all samples are considered unacceptable when compared against the commonly accepted standard for ship models (ie. equivalent to that achieved with a 300 to 400 grit wet and dry paper). Additional processes, such as sanding and sealing, may be required prior to performing model tests. The surface roughness of the test samples produced using rapid prototyping and several ship models constructed of various materials, were quantified by direct measurement using a commercially available surface roughness tester. A chart for estimating the effect of surface roughness on resistance is provided.

13.5 Task 8

Recent advances regarding turbulence stimulation methods have been reviewed. Given the wide variation in model geometry the turbulence stimulator device should be chosen following consideration of its effectiveness and convenience for the individual purpose. The need to carefully consider the specific type, size, quantity and placement of turbulence stimulator device has been further emphasised within the relevant procedure 7.5-01-01-01 Ship Models. Particular attention was given to model tests on long slender hulls, such as high speed catamarans, where the use of sand strips are recommended. Additional advice on the approach for selecting appropriate turbulence stimulation devices for appendages is provided. Two ways are typically used to determine the efficiency of tripping devices. The assessment of the flow past the stimulators (usually done using hot-film sensors) or the evaluation of the drag force at a particular speed for different stimulation devices. If used correctly, all three commonly used devices (studs, sand strips and trip wires) are capable of tripping the flow around ship or submarine models without causing notable parasitic drag or over-stimulating the boundary layer.

13.6 Tasks 7 & 11

The results of the small model campaign have been included for completeness, but the RC don't think there is any insight to be gained from looking at the small model results themselves and the major conclusions from the worldwide campaign were from the large model and presented in the 27th ITTC RC final report. It is believed that there is little further to gain from additional analysis of the worldwide series benchmark data.

13.7 Task 10

The ITTC benchmark study on PIV and SPIV measurements has been initiated. Clear instructions for performing the benchmark tests including details about the case studies, the measurement conditions and the measurement parameters have been included in the revised 7.5-01-03-04 procedure. The organization of the benchmark program along with all the necessary information to access the repository and to store the data are also reported in the revised 7.5-01-03-04 procedure.

13.8 Potential New Tasks

- Conduct a study of super-hydrophobic materials from the point of view of resistance reduction.

- Accumulate and classify the original benchmark test data listed in the revised ITTC procedure 7.5-03-02-02 "Benchmark Database for CFD Validation for Resistance and Propulsion", working closely with other ITTC committees and CFD workshop commit-

tees. Make the database available on the ITTC website and encourage continual improvement of the data.

- Produce guidelines on the verification of ship scale CFD, by checking model to ship scaling of skin friction, form factor and wave resistance components. Review and update uncertainty analysis guidelines for CFD.

14 REFERENCES

Akbarzadeh, P., Molana, P., and Badri, M. A. 2015, "Determining resistance coefficient for series 60 vessels using numerical and experimental modelling," Ships and Offshore Structures, 11(8):874-879.

Arun K. Kota, Gibum Kwon, Wonjae Choi, Joseph M. Mabry, and Anish Tuteja 2012, "Hygro-responsive membranes for effective oil-water separation," Nature Communications, 3:1025, DOI: 10.1038/2027. (Impact Factor: 7.396),

Atlar, M., Bashir, M., Turkmen, S., Yeginbayeva, I., Carchen, A., Politis, G., 2015, "Design, manufacture and operation of a strut system deployed on a research catamaran to collect samples of dynamically grown biofilms in-service," Proceedings of 4th International Conference on Advanced Model Measurement Technology for the Maritime Industry (AMT'15), Istanbul,.

Banner, M. L. and Peregrine, D. H., 1993, "Wave breaking in deep water," Annual Review of Fluid Mechanics, 25:373-397.

Bennett, S. S., Downes, J., Phillips, A. B., & S. R., T., 2015, "Rapid prototyping of flexible models-a new method for model testing?" Paper presented at the 7th International Conference on Hydroelasticity in Marine Technology.

Bertram, V., 2000, Practical Ship Hydrodynamics, Butterworth Heinemann.

Binns, J. R., Albina, F. O., and Burns, I. A., 2009, "Looking for 'laminars': Measuring intermittency on the America's Cup race course," Experimental Thermal and Fluid Science, 33(5):865-874.

Bojovic, P., 1998, "Resistance prediction of high speed round bilge hull forms," Masters Thesis, Australian Maritime College.

Bradford, D., 2015, "Transitional flow around wave-piercing catamaran hulls using experimental techniques," BEng Thesis, Australian Maritime College, University of Tasmania.

Braslow, A. L., Hicks, R. M., and Harris, R. J. V., 1966, "Use of grit-type boundary-layer-transition trips on wind-tunnel models," NASA Technical Note N66 36119.

Breslin, J. P. and Macovsky, M. S., 1950, "Effects of turbulence stimulators on the boundary layer and resistance of a ship model as detected by hot wires," David W. Taylor Model Basin, report 724.

Brouwer, J. and Klinkenberg, Y. J., 2016, "Examining random uncertainty using a newly developed power spectrum based method," Proceedings of the ASME 2016 35th International Conference on Ocean, Offshore and Arctic Engineering, 35.

Cho, S.-R., Ha, J.-S., Jeong, S.-Y., and Kang, K.-J., 2015, "Study on friction characteristics between ice and various rough plates," Proceedings of the ASME 2015 34th International Conference on Ocean, Offshore and Arctic Engineering.

Compton, R. H., 1986, "Resistance of a Systematic Series of Semiplaning Transom-Stern Hulls," Marine Technology, 23(4):345-370.

Dai, Z., W.-H. Chou, and G.M. Faeth, "Drop formation due to turbulent primary breakup at the free surface of plane liquid wall jets," Physics of Fluids, 10(5), 1147-1157, 1998.

Davidson, K. S. M., 1951, "Turbulence Stimulation in Model Test," International Towing Tank Conference.

Day, A. H., Clelland, D., and Doctors, L. J. , 2009, "Unsteady finite-depth effects during resistance tests on a ship model in a towing tank," Journal of marine science and technology, 14(3):387-397.

Delen, C. and Bal, S., 2015, "Uncertainty analysis of resistance tests in Ata Nutku ship model testing laboratory of Istanbul Technical University," Proceedings of the 16th Congress of IMAM, Pula, Croatia, 21-24 September, pp: 43-50

Demirel, Y. K., Khorasanchi, M., Turan, O., Incecik, A., and Schultz, M. P., 2014, "A CFD model for the frictional resistance prediction of antifouling coatings," Ocean Engineering, 89:21-31.

Demirel, Y.K., Turan, O., Day, S., 2015, "Experimental determination of added hydrodynamic resistance caused by marine biofouling on ships," Proceedings of 4th International Conference on Advanced Model Measurement Technology for the Maritime Industry (AMT'15), Istanbul.

Demirel, Y. K., Turan, O., and Incecik, A., 2016, "Predicting the effect of biofouling on ship resistance using CFD," Applied Ocean Research.

Denny, M. E. and Maurice, S. E., 1951, "BSRA Resistance Experiments on the ' Lucy Ashton' , Part I Full scale measurements," TINA.

Dong, R. R., Katz, J., and Huang, T. T., 1997, "On the structure of bow waves on a ship model," J. Fluid Mech., 346:77-115.

Eslamdoost, A., 2014, "The Hydrodynamics of Waterjet/Hull Interaction," Chalmers University.

Falchi, M., Felli, M., Grizzi, S., Aloisio, G., Broglia, R. and Stern, F., 2016, "Stereo Piv Measurements for The Delft 372 Catamaran Advancing In Steady Drift Conditions," Chapter 5 of "Reliable Prediction of Separated Flow Onset and Progression for Air and Sea Vehicles", 227-270. STO-TR-AVT-183, DOI: 10. 14339/ST O-TR-AVT-183, ISBN: 978-92-837-2089-8.

Fu, T.C., Bardet, P.M, Hackett, E.E., and Kowalski, A., "On the break-up of a turbulent liquid wall sheet," 18th Australasian Fluid Mechanics Conference, Launceston, Australia, December 3-7. 2012.

Gao, Z., Yang, H., and Pang, Q., 2014, "Prediction of ship resistance in muddy navigation area using RANSE," Advanced Engineering and Technology: Proceedings of the 2014 Annual Congress on Advanced Engineering and Technology.

Gao, Z., Yang, H., and Xie, M., 2015, "Computation of Flow around Wigley Hull in Shallow Water with Muddy Seabed," Journal of Coastal Research, 73:490-495.

Gillmer, T. C. and Johnson, B., 1982, Introduction to Naval Architecture. Naval Institute Press.

Guiard, T., Leonard, S., and Mewis, F., 2013, "The Becker Mewis duct-challenges in full-scale design and new developments for fast ships," Proceedings of Third International Symposium on Marine Propulsors.

Ginnis, A., Duvigneau, R., Politis, C., Kostas,

K., Bellibassakis, K., Gerostathis, T., and Kaklis, P., 2013, "A Multi-Objective Optimization Environment for Ship-Hull Design Based on a BEM-Isogeometric Solver," Proceedings of 5th International Conference on Computational Methods in Marine Engineering.

Gourlay, T. P., Ha, J. H., Mucha, P., and Uliczka, K., 2015, "Sinkage and Trim of Modern Container Ships in Shallow Water." Australasian Coasts & Ports Conference.

Haase, M., Binns, J., Thomas, G., and Bose, N., 2016c, "Wave-piercing catamaran transom stern ventilation process," Ship Technology Research-Schiffstechnik, 63(2).

Haase, M., Binns, J., Bose, N., Davidson, G., Thomas, G., and Friezer, S., 2015, "Hydrodynamic hull form design space exploration of large medium-speed catamarans using full-scale CFD," Trans RINA, Intl J Maritime Eng, 157(A3).

Haase, M., Davidson, G., Binns, J., Thomas, G., and Bose, N., 2016a, "Full-scale resistance prediction in finite waters: A study using computational fluid dynamics simulations, model test experiments and sea trial measurements," Proc IMechE Part M: J Engineering for the Maritime Environment.

Haase, M., Zurcher, K., Davidson, G., Binns, J. R., Thomas, G., and Bose, N., 2016b, "Novel CFD-based full-scale resistance prediction for large medium-speed catamarans," Ocean Engineering, 111:198-208

Hagesteijn, G., Hooijmans, P., and van der Meij, K., 2016, "Correlation allowances in model tests results: a delicate balance between performance, accuracy and commercial interests?" Proceedings of the ASME 2016 35th International Conference on Ocean, Offshore and Arctic Engineering.

Hackett, E.E., Carneal, J., Pfitsch, D., Fullerton, A.M., Walker, D., Fu, T.C., Wyatt, D.C., O' Shea, T.T., Brucker, K., & Dommermuth, D. G., "An experimental and numerical study on the break-up of a turbulent liquid wall sheet," Proceedings of the 29th Symposium on Naval Hydrodynamics, 2012.

Havelock, T., 1949, "The wave resistance of a cylinder started from rest," The Quarterly Journal of Mechanics and Applied Mathematics, 2(3):325-334.

Hughes, G. and Allan, J. F., 1951, "Turbulence stimulation on ship models," Summer meeting of The Society of Naval Architects and Marine Engineers.

Hutchison, C., 2014, "The use of hot-films to characterize flow regimes on a sailing yacht hull-guidance for scaling," PhD Thesis, Australian Maritime College, University of Tasmania.

ITTC 2002, "Uncertainty Analysis, Example for Resistance Test," ITTC Recommended Procedures and Guidelines, Procedure 7.5-02-02-02, Revision 01.

ITTC 2011 "Report of Resistance Committee," Proceedings of the 26th International Towing Tank Conference, Rio de Janeiro, Brazil.

ITTC 2014, "Final Report and Recommendations to the 27th ITTC by Resistance Committee," Proceedings of the 27th ITTC Full Conference, August 31-September 5, Copenhagen, Denmark

ITTC 2014, "Practical Guide for Uncertainty Analysis of Resistance Measurement in Routine Tests," ITTC Procedure7.5-02-02-02.2.

Jones, M. B., Erm, L. P., Valiyff, A., and Henbest, S. M., 2013, "Skin-Friction Measurements on a Model Submarine," DSTO-TR-

2898.

Kamal, I. M., Zurcher, K., Bose, N., Binns, J., Chai, S., and Davidson, G., 2015, "Powering for Medium Speed Wave-Piercing Catamarans comparing Waterjet and Screw Propeller Performance using Model Testing," Proceedings of Fourth International Symposium on Marine Propulsors.

Kinaci, O.K, Sukas, O.F. and Bal, S., 2016, "Prediction of wave resistance by a Reynolds-averaged Navier-Stokes equation-based computational fluid dynamics approach," Proceedings of the Institution of Mechanical Engineers, Part M, Journal of Engineering for the Maritime Environment, 230(3): 531-548.

Kleinsorge, L., Lindner, H., and Bronsart, R., 2016, "A Computational Environment for Rapid CFD Ship Resistance Analyses," Proceedings of PRADS.

Lee, K., 2014, "Tackling the Laminar-Turbulent Transition at Medium-Speed Catamarans Using Computational Fluid Dynamics," BEng Thesis, Australian Maritime College, University of Tasmania.

Li, C., Skiadaresis, D., Politis, G., Yeginbayeva, I., Atlar, M., Burgess, G., Thomason, J.C., 2015, "Drag tests on foul-release coatings with biofilm using an axysmmetric testing body," Proceedings of 4th International Conference on Advanced Model Measurement Technology for the Maritime Industry (AMT'15), Istanbul.

Lin, S. P., and R. D. Reitz, "Drop and spray formation from a liquid jet," Annual Review Fluid Mechanics, 30, 85-105, 1998.

Lindholdt, A., Dam-Johansen, K., Olse, S. M., Yebra, D. M., and Kiil, S., 2015, "Effects of biofouling development on drag forces of hull coatings for ocean-going ships: a review," J. Coat. Technol. Res., 12(3):415-444.

Liu, T., 2013, "Extraction of skin-friction fields from surface flow visualizations as an inverse problem," Meas. Sci. Technol. 24(12), 12400.

Luca, F. D., Mancini, S., Miranda, S., and Pensa, C., 2016, "An Extended Verification and Validation Study of CFD Simulations for Planing Hulls," Journal of Ship Research, 60 (2):101-118.

Manen, J.D.van, Oossanen, P. van, 1988, "Resistance and Propulsion of Ships," Principles of Naval Architecture Vol. II.

McCarthy, J. H., Power, J. L., and Huang, T. T., 1976, "The roles of transition, laminar separation and turbulence stimulation in the analysis of axisymmetric body drag," Proceedings of the Eleventh Symposium on Naval Hydrodynamics, page 69-95.

McDonagh, G., 2016, "Experimental determination of turbulence stimulator design on a wave-piercing catamaran scale model," BEng Thesis, Australian Maritime College, University of Tasmania.

Mikkelsen, H. and Steffensen, M. L., 2016, "Full scale validation of CFD model of self-propelled ship," Master Thesis Technical University of Denmark.

Molland, A.F., Wellicome, J.F., and Couser,P. R., 1994, "Resistance Experiments on a Systematic Series of High Speed Displacement Catamaran Forms: Variation of Length-Displacement Ratio and Breadth-Draught Ratio," Ship Science Report 71, University of Southampton (http://eprints. soton. ac. uk/ 46442/)

Monty, J. P., Dogan, E., Hanson, R., Scardino, A. J., Ganapathisubramani, B., and Hutchins, N., 2016, "An assessment of the ship drag

penalty arising from light calcareous tubeworm fouling," Biofouling, 32(4):451-464.

Mucha, P., Deng, G., Gourlay, T. P., and El Moctar, O., 2016, "Validation studies on numerical prediction of ship squat and resistance in shallow water," Proceedings of MASHCON, pages 122-133.

Murphy, J. C., 2010, "A novel approach to turbulence stimulation for ship-model testing," Tech Report U.S. Naval Academy no. 390.

Olivieri, A., Pistani, F., Avanzini, A., Stern, F. and Penna, R., 2001, "Towing Tank Experiments of Resistance, Sinkage and Trim, Boundary Layer, Wake, and Free Surface Flow Around A Naval Combatant Insean 2340 Model," IIHR Technical Report No. 421, September, Iowa City, Iowa, USA.

Olson, D., Naguib, A., and Koochesfahani, M., 2015, "Measurement of the wall pressure and shear stress distribution using molecular tagging diagnostics," Exp. Fluids 56(8), 1-6.

Ozdemir, Y. H., Barlas, B., Yilmaz, T., and Bayraktar, S., 2014, "Numerical and experimental study of turbulent free surface flow for a fast ship model," Brodogradnja/Shipbuilding, 65(1).

Pan, S., Kota, A.K., Mabry, J., and Tuteja, A. 2013, "Superomniphobic surfaces for effective chemical shielding," Journal of the American Chemical Society, 2013, 135 (2), 578-581 (Impact Factor: 9.907).

Patel, P. K. and Premchand, M., 2015, "Numerical investigation of the influence of water depth on ship resistance," International Journal of Computer Applications, 116(17): 10-17.

Pattenden, R.J., Bressloff, N.W., Turnock, S.R. and Zhang, X., 2007, "Unsteady simulations of the flow around a short surface-mounted cylinder," International Journal for Numerical Methods in Fluids, 53, (6), 895-914.

Pattenden, R.J., Turnock, S.R. and Zhang, X., 2005, "Measurements of the flow over a low-aspect-ratio cylinder mounted on a ground plane," Experiments in Fluids, 39, (1), 10-21.

Pearson, M., 2015, "Modelling laminar-turbulent transition on wave-piercing catamarans for enhancing experimental techniques," BEng Thesis, Australian Maritime College, University of Tasmania.

Peregrine, D. H. and Svedsen, I. A., 1978, "Spilling breakers, bores and hydraulic jumps," Proc. 16th Coastal Engineering Conf. ASCE, page 540-550.

Perelman, O., Vermare, J., Darquier, M., Perdon, P., 2015, "Skin friction local measurements at high Reynolds number at DGA hydrodynamics," Proceedings of 4th International Conference on Advanced Model Measurement Technology for the Maritime Industry (AMT'15), Istanbul.

Ponkratov, D., 2016, "A workshop on ship scale hydrodynamic computer simulation," Lloyd's Register.

Ponkratov, D. and Zegos, C., 2015, "Validation of ship scale CFD self-propulsion simulation by the direct comparison with sea trials results," Proceedings of 4th International Symposium on Marine Propulsors.

Preston, J. H., 1958, "The minimum Reynolds number for a turbulent boundary layer and the selection of a transition device," Journal of Fluid Mechanics, 3.04:373-384.

Roth, G. I., Mascenik, D. T., and Katz, J., 1999, "Measurements of the flow structure and turbulence within a ship bow wave," Physics of Fluids, 11(11):3512-3523.

Rovere, J. E., 1997, "Catamaran resistance from tests on a single demihull," Proc. 4th Intl Fast Sea Transportation Conference.

Sarpkaya, T., and C. F. Merrill, "High speed laser-PIV imaging for the Eulerian-Lagrangian measurement and visualization of spray on wall-bounded jets," 8th International Conference on Liquid Atomization and Spray Systems, Pasadena, CA, 2000.

Savio L., Berge B.O., Koushan K., Axelsson M., 2015, "Measurements of added resistance due to increased roughness on flat plates," Proceedings of 4th International Conference on Advanced Model Measurement Technology for the Maritime Industry (AMT'15), Istanbul.

Schlichting, H. and Gersten, K., 2000, Boundary Layer Theory, Springer.

Schnabel, P., 2017, "Impact of laminar flow on viscous drag of wave-piercing catamarans at model scale," Conjoint BEng Thesis, Universität Rostock and Australian Maritime College, University of Tasmania.

Schultz, M. P., Walker, J. M., Steppe, C. N., and Flack, K. A., 2015, "Impact of diatomaceous biofilms on the frictional drag of fouling-release coatings," Biofouling, 31(9-10): 759-773.

Shakeri, M., Tavakolinejad, M. and J.H. Duncan, "An experimental investigation of divergent bow waves simulated by a two-dimensional plus temporal wave marker technique," J. Fluid Mechanics, 634, pp. 217-243, 2009.

Shen, Y. T. and Hess, D. E., 2011, "A method to scale the roughness of submarine nonskid coatings on a free-running model for maneuvering experiments," Journal of Ship Research, 55(1):64-69.

Shen, Y. T., Hughes, M. J. and Gorski, J. J., 2015, "Resistance prediction on submerged axisymmetric bodies fitted with turbulent spot inducers," Journal of Ship Research, Vol. 59, No. 2, June, pp. 85-98.

Sherbaz, S. and Duan, W., 2014, "Ship trim optimization: Assessment of influence of trim on resistance of MOERI container ship," The Scientific World Journal.

Smits, A. J., 1982, "Turbulence stimulation and the initial boundary-layer development on two ship forms," Journal of Ship Research, 26(3):166-175.

Steen, S., Ankit, and Gavrilin, S., 2015, "Uncertainty analysis in ship-model resistance test," Proceedings of the ASME 2015 34th International Conference on Ocean, Offshore and Arctic Engineering, 34.

Sun, J., Tu, H., Chen, Y., Xie, D., and Zhou, J. 2016, "A study on trim optimization for a container ship based on effects due to resistance," J. of Ship Research, 60(1):30-47.

Tezdogan, T., Incecik, A., and Turan, O., 2016, "A numerical investigation of the squat and resistance of ships advancing through a canal using CFD," J Mar Sci Technol, 21:86-101.

Tsubogo, T., 2016, "Near field expression of ship wave resistance by green's theorem," Proceedings of the ASME 2016 35th International Conference on Ocean, Offshore and Arctic Engineering.

Turan, O., Demirel, Y. K., Day, S., and Tezdogan, T., 2016, "Experimental determination of added hydrodynamic resistance caused by marine biofouling on ships," Proceedings of 6th Transport Research Arena, 14:1649-1658.

Vargas, A. and Shan, H., 2016, "A numerical

approach for modelling roughness for marine applications," Proceedings of ASME 1st Symposium on Marine Hydrodynamics.

Walker, J. M., Schultz, M. P., Flack, K. A., and Steppe, C. N., 2014, "Skin-friction drag measurements on ship hull coating systems," Proceedings of 30th Symposium on Naval Hydrodynamics.

Wehausen, J. V., 1964, "Effect of the initial acceleration upon the wave resistance of ship models," Journal of Ship Research, 7(3):38-50.

White, F. M., 2009, Fluid Mechanics. McGraw Hill.

Will, J. and Kompe, A., 2015, "Improvements in the prediction of the wave making resistance from potential flow by using transverse wave cut methods," Proceedings of the ASME 2015 34th International Conference on Ocean, Offshore and Arctic Engineering.

Zurcher, K., 2015, "Waterjet testing techniques for powering performance estimation using a single catamaran demihull," Doctor of Philosophy thesis, Australian Maritime College, University of Tasmania.

Zurcher, K., Bose, N., Binns, J. R., Thomas, G., and Davidson, G., 2013, "Design and commissioning tests for waterjet self-propulsion testing of a medium-speed catamaran ferry using a single demihull," Proceedings of Third International Symposium on Marine Propulsors.